J. Fluid Mech. (2002), *vol.* 450, *pp.* 97–130.
DOI: 10.1017/S002211200100622X Printed in the United Kingdom

Experimental investigation of density fluctuations in high-speed jets and correlation with generated noise

By J. PANDA[1,2] AND R. G. SEASHOLTZ[2]

[1]Ohio Aerospace Institute, Cleveland, OH 44142, USA

[2]NASA Glenn Research Center, Cleveland, OH 44135, USA

(Received 28 August 2000 and in revised form 2 January 2001)

The air density fluctuations in the plumes of fully expanded, unheated free jets were investigated experimentally using a Rayleigh-scattering-based technique. The point measuring technique used a continuous-wave laser, fibre-optic transmission and photon counting electronics. The radial and centreline profiles of time-averaged density and root-mean-square density fluctuation provided a comparative description of jet growth. To measure density fluctuation spectra a two-photomultiplier-tube (PMT) technique was used. Cross-correlation between the two PMT signals significantly reduced the electronic shot noise contribution. The density fluctuation spectra were found to be remarkably similar for all Mach number jets. A detailed survey in fully expanded Mach 0.95, 1.4 and 1.8 jets further confirmed that the distribution of various Strouhal frequency fluctuations remained similar, except for a spatial stretching with increased Mach number. In spite of this similarity in flow fluctuations the noise sources in these three jets were found to be significantly different. Spark schlieren photographs and near-field microphone measurements confirmed that Mach wave radiation was present in the Mach 1.8 jet, and was absent in the Mach 0.95 jet. Direct correlation measurement between the flow density fluctuation (cause) and far-field sound pressure fluctuation (effect) shed further light on the sound generation process. For this purpose a microphone was kept fixed at a far-field point, mostly at a distance of 50 diameters and 30° to the flow direction, and the laser probe volume was moved from point to point in the flow. In the Mach 1.8 jet, where the convective velocity of Kelvin–Helmholtz instability waves exceeded the ambient sound speed, significant correlation was measured from the peripheral shear layer, while in the Mach 0.95 jet, where the instability waves had subsonic convective speed, no correlation could be measured. Although the same instability waves were present in both Mach 1.8 and 0.95 jets, the peripheral shear layer of the former was found to be an obvious noise source, while that of the latter was not. Further correlation studies along the jet centreline showed that behaviour in the region downstream of the potential core was similar in all Mach number jets tested, $0.6 \leqslant M \leqslant 1.8$. Good correlation at low Strouhal frequencies was measured from this region, which started from downstream of the potential core and extended many diameters from there.

1. Introduction

The closing of the High Speed Civil Transport (HSCT) program in the USA has pointed out the technological advances needed in this arena for the success of a future

supersonic, civilian aircraft. In addition, more stringent government and community requirements for aircraft noise are creating a further challenge to reduce noise emission from the current subsonic fleet. So far various experimental efforts depend on a 'cut-and-try' approach, where one primarily looks for a change in the far-field sound spectrum after making a new nozzle. A more science-based approach is to look for a change in the noise sources and therein lays the present difficulty. Since turbulence fluctuations in the jet are the source of sound, source modelling is as good as our knowledge of the turbulence. On the theoretical front there exist multiple formulations. The most prominent one is based on the acoustic analogy approach of Lighthill (1954), Lilley (1972) and others. In spite of its elegance, the sound source description is complex and direct measurement of the source terms has remained an unattainable goal. Recent direct numerical simulations (DNS) (Freund 2001; Colonius, Lele & Moin 1997) have successfully quantified the Lighthill stress tensor and the quadrupole sources, albeit for a simple geometry and very low Reynolds number. Early aerodynamic noise theories modelled the source terms assuming turbulence to be made up of small-scale random eddies with a Gaussian form of correlation function (Ffowcs Williams 1963). With the realization that turbulence is not all small random eddies, but includes long coherent fluctuations due to the hydrodynamic instability waves (Mollo-Christensen 1967; Crow & Champagne 1971; Moore 1977 among others), new theoretical formulations of the sound sources emerged. Michalke (1970, 1972) used the framework of Lighthill's integral formulation but expanded the sources in wave-type terms to describe the effects of instability waves. Morris & Tam (1979) and Tam & Burton (1984) deviated from the acoustic analogy route and matched the pressure field of instability waves, obtained through a linearized Euler's equation, to the far-field acoustic pressure through a matched asymptotic expansion. Their analysis drew heavily on the experimental work on low Reynolds number jets by McLaughlin, Morrison & Trout (1975) and Morrison & McLaughlin (1979) who measured the properties of instability waves and their noise radiation characteristics in supersonic jets. The instability wave based approach has been successful in predicting noise emitted at low angles to the jet axis from supersonic streams. However, the noise radiation for all other angles in supersonic jets, the noise field of subsonic jets, and the high-frequency part of the acoustic spectra in a jet at any Mach number could not be explained.

Experimentally, the problem of source identification is twofold. First, a reliable tool to measure unsteady turbulence in compressible flow is unavailable. While the theoretical approaches require a thorough knowledge of complex turbulence properties, even simple turbulence statistics for compressible flows are difficult to measure. Smits & Dussauge (1996), in a recent book on turbulent shear layers, write: 'The form of spectrum in compressible turbulence is still unknown'. The present work takes on the task of measuring turbulence spectra, specifically density fluctuation spectra, using a Rayleigh scattering based technique. The second problem of source identification is the difficulty in ascertaining that the measured flow fluctuation is truly creating far-field acoustic radiation. The present work uses a direct correlation study 'between the cause and the effect' (Lee & Ribner 1972; Siddon & Rackl 1972), that is, between the turbulent density fluctuation and far-field noise, to locate noise sources. Our goal is therefore twofold: first, to provide a reliable and accurate database that can be used to validate computational aeroacoustics codes; second, to locate and determine the relative strength of various sound sources experimentally in a high Reynolds number jet.

The bulk of the correlation study was for a microphone location of 30° to the flow direction, where noise from instability waves is known to dominate. Therefore, the

present work primarily discusses the role of instability waves in the sound generation process. The experimental results were not tied to any theory. It should be pointed out that density as a sound source in Lighthill's equation can be thought of in two different ways. Lighthill's equation is

$$\partial^2\rho/\partial t^2 - a_0^2\nabla^2\rho = \partial^2 T_{ij}/\partial x_i \partial x_j, \quad T_{ij} = \rho u_i u_j + \delta_{ij}(p - a_0^2\rho),$$

where ρ is air density, p pressure, a_0 ambient sound speed, and u_i velocity vector. The first description is through the right-hand side, via an acoustic analogy interpretation. Here density appears in both quadrupole and dipole terms of T_{ij}, none of which can be neglected in supersonic jet flows. The second description is through the left-hand side via the D'Alambertian of density. If $\partial^2\rho/\partial t^2 - a_0^2\nabla^2\rho$ can be measured everywhere in the flow, that will be equivalent to measuring the sum of the dipole and quadrupole terms on the right (Freund 2001).

The lack of experimental data in compressible jets is primarily due to various problems in using traditional experimental tools. In the past, dynamic measurements in compressible jets were attempted using hot-wire probes or laser Doppler velocimetry (LDV). The success of using hot wires by McLaughlin *et al.* (1975) and Morrison & McLaughlin (1979) is attributed to the very low Reynolds number operation of their jet. At higher Reynolds numbers, hot wires are prone to breakage. At mixed subsonic and supersonic operating conditions, the analysis of hot-wire signals becomes intractable. Armstrong, Michalke & Fuchs (1977) used intrusive microphones in Mach 0.7 jets to measure pressure fluctuation spectra. They have described a problem of standing wave formation in the jet that worsens with increasing Mach number. LDV, along with a high seeding rate, has been used (Lau 1981; Jiang & Sislian 1998, among others) to determine velocity fluctuation statistics. However, various problems associated with seed particles following the flow, severe biasing problems in turbulent shear flows and difficulties in measuring spectra cast doubt on such data. Currently, particle image velocimetry (PIV) is extensively used to measure time-averaged velocity fields. The extension of this technique to dynamic spectral measurement is yet to be done. Still, problems, similar to that found with LDV, are expected to persist. In the present program a laser-based, non-intrusive Rayleigh scattering technique that depends on light scattering from air molecules is used. Since there are no particles, many problems associated with LDV and PIV can be overcome. Wilson & Damkevela (1970) used a non-intrusive crossbeam technique to measure mean-square density fluctuations. Some of their results are compared with similar data obtained from the present study. The crossbeam technique was also used to correlate density fluctuations to far-field sound pressure fluctuations (Damkevala, Grosche & Guest 1973, among others). However, the fundamental assumption of homogeneous turbulence, used in the crossbeam technique, is invalid in a jet.

Based on Proudman's (1952) analysis, the above-mentioned causality approach of relating flow fluctuations to the far-field noise was taken by many researchers. In this method, the velocity, density or pressure fluctuations in the jet were correlated with the sound pressure fluctuation measured by a microphone. The primary problem of all of these efforts is with the flow fluctuation measurement. The noise produced by intrusive hot-wire probes (Seiner & Reethof 1974 and others) or microphones placed inside the flow (Hurdle, Meecham & Hodder 1974 and others) contributed most of the correlation in some experiments. Later on, LDV was used by Schaffer (1979) and Richarz (1979) among others. Schaffer wrote down the vast number of approximations and assumptions needed to relate the experimental data to theory. Nevertheless, an important issue of accuracy in velocity spectra measurements using

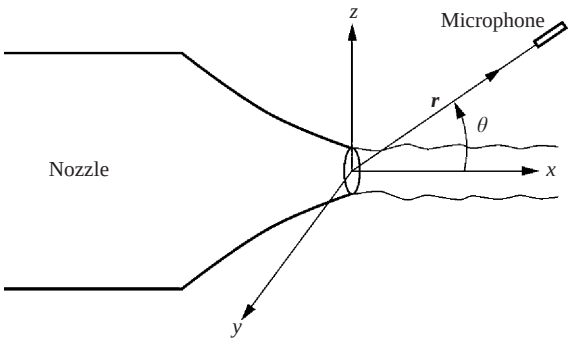

FIGURE 1. The coordinate system.

LDV was not answered. Before attempting to measure correlation, it is natural to expect that the individual components would be measured accurately. This important step, however, was skipped. A significant part of the present work concentrates on this aspect before attempting a correlation measurement. It is interesting to note Ffowcs Williams' (1973) evaluation report on a host of experimental papers at the 1973 AGARD conference on Noise Mechanism: 'Many papers presented at the Specialist Meeting dealt with different aspects of source location but none of them faced up to the difficult issue of interpreting or speculating on the degree of ambiguity that must inevitably be contained in the experimental results'.

The paper places particular emphasis on the measurement technique, and a detailed description is provided in the following experimental set-up section. The fluid dynamics and aeroacoustics results are separately discussed in the results and discussion section.

2. Experimental set-up

Experiments were performed at NASA Glenn Research Center using three different nozzles (one convergent and two convergent–divergent) operated at Mach numbers, $M = 0.95$, 1.4 and 1.8. The convergent–divergent nozzles were designed by the method of characteristics and their geometries were reported in Panda & Seasholtz (1999*a*). All nozzles were 25.4 mm in exit diameter. The jet facility used a continuous supply of unheated compressed air. The facility was located in a large test chamber, which was not anechoic *per se*, but acoustic absorbent material was placed around the vicinity of the nozzle and in the ceiling and walls of the test cell to minimize reflection. Two 1/4 in. microphones with the 'protection grid' removed were used to measure sound pressure fluctuation spectra. The coordinate system used throughout this paper is shown in figure 1. The traversing system allowed flow measurements in the horizontal (x, y)-plane. The microphones were placed in the vertical (x, z)-plane to minimize the effect of reflection from the large optical lenses and beam traps. Whenever possible, various parts of the optical train, air supply duct and jet facility were covered by either 1/2 or 1/4 in. thick polyurethane foam. However, the uncovered optical surfaces in the jet vicinity remained acoustic reflectors. The Rayleigh scattering system is quite elaborate and the following provides a description.

2.1. *Laser Rayleigh scattering*

When a laser beam is allowed to pass through a gas, the molecules present in the gas cause inelastic and elastic light scattering. The inelastic part is called Raman scattering

and the elastic part Rayleigh scattering. The Raman scattering cross-section is far weaker than the Rayleigh scattering one; typically for room-temperature nitrogen, vibrational and rotational Raman scattering contribute, respectively, 0.1% and 1% of the total scattered light. Therefore, the elastic Rayleigh scattering process describes most of the scattered light. For gas density measurement, variation of the total light intensity with the molecular number density is of interest. Since this variation is identical for both the Rayleigh and Raman scattering process, a separation between the two is unnecessary. The following considers the Rayleigh scattered part where the scattered light, P_s, collected from a probe volume, V_{sc} into a solid angle, $\mathrm{d}\Omega$, can be written as (Seasholtz, Zupanc & Schneider 1992)

$$P_s = mI_0 V_{sc} \frac{\mathrm{d}\sigma}{\mathrm{d}\Omega} \sin^2 \chi \mathrm{d}\Omega = k'm. \tag{1}$$

Here m is the molecular number density, I_0 is the incident light intensity, $\mathrm{d}\sigma/\mathrm{d}\Omega$ is the differential Rayleigh scattering cross-section of the gas (or gas mixture) under consideration and χ is the angle between the incident electric vector and the direction of light collection. The Rayleigh scattering cross-section depends on the light wavelength and the effective molecular diameter. This is constant for a fixed-wavelength laser and a fixed gas mixture (air for this work). For a fixed optical set-up, the scattered laser power is directly proportional to the molecular number density. Now, the number density m, is related to the bulk density, ρ through the following:

$$m = \frac{\rho N_A}{M}, \tag{2}$$

where M is the molecular weight and N_A is the Avogadro constant ($6.022 \times 10^{26}\,\mathrm{kmole}^{-1}$). The scattered light intensity was measured using a photomultiplier tube and a photon counting process was performed. The number of photons collected during a fixed time interval Δt can be written as

$$N = \frac{\varepsilon P_s \Delta t}{hv} = \frac{\varepsilon \rho N_A I_0 V_{sc} \dfrac{\mathrm{d}\sigma}{\mathrm{d}\Omega} \sin^2 \chi \mathrm{d}\Omega \Delta t}{Mhv} = k\rho \Delta t, \tag{3}$$

where h is the Planck constant, v is the frequency of the laser light and ε is the overall collection efficiency (a product of the light transmission efficiency and the quantum efficiency of the photomultiplier tube). Equation (3) shows that the photon count over a fixed time interval is directly proportional to the gas density at the probe volume. The proportionality constant k has to be determined through a calibration process.

Figure 2 shows a schematic of the free air jet facility and the Rayleigh scattering set-up. The point measurement technique used a continuous wave (CW) laser beam focused to a point in the flow, with the molecular scattered light collected and measured using photomultiplier tubes (PMT). The green laser light (532 nm wavelength) from a CW, single-frequency, frequency-doubled Neodymium Vanadate ($\mathrm{Nd} : \mathrm{YVO_4}$) laser was transferred to the jet vicinity by a 0.365 mm-core-diameter, multi-mode optical fibre and focused to a probe volume. Light scattered by the air molecules was collected at an 85° scattering angle and focused on the face of a 0.55 mm-core-diameter multi-mode optical fibre. The combination of focusing and imaging optics makes the probe volume length equal to 1.03 mm. The complete transmitting and receiving optics were mounted on an x, y traverse that allowed the probe volume to be moved automatically over a plane. A more detailed description of the optical components can be found in Panda & Seasholtz (1999*b*). The scattered light, collected by the receiving fibre, was transmitted to a quiet neighbouring room away

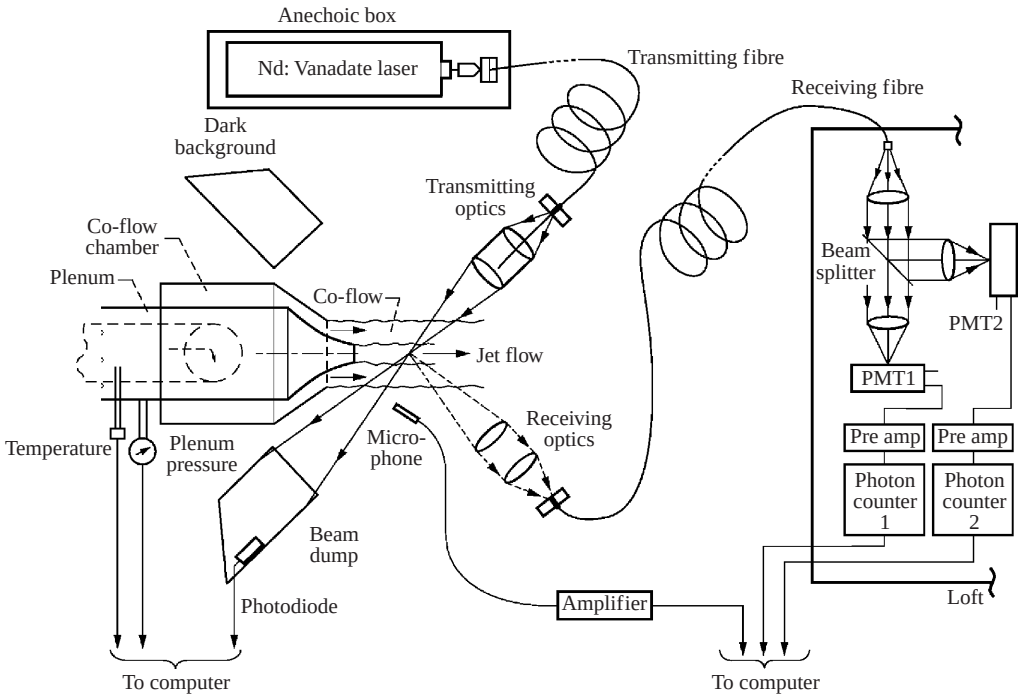

FIGURE 2. Schematic of jet facility and Rayleigh scattering set-up.

from the noisy environment. Here the collected light was collimated and then split into two equal parts by a thin-film beam splitter. Each of the beams was refocused into individual photomultiplier tubes. Photon counting electronics were then used to measure light intensities. The advantage of the photon counting approach over the conventional measurement of analogue PMT output (Pitts & Kashiwagi 1984; Gouldin & Halthore 1986) is a clearer estimate of measurement uncertainty due to electronic shot noise. The counting was performed over a series of contiguous time bins of specified interval. The maximum number of bins that can be used at a time was 16 384. Usually, multiple sets of data were collected and passed to a Personal Computer. The timer cycle for bin width was supplied externally through a programmable signal generator. All analogue signals (from microphone amplifiers and pressure transducers indicating plenum and ambient conditions) were digitized and passed to the same computer. The data collection process was automated to move the laser probe volume from point to point in the flow field, perform the photon-counting process and collect the time history. When needed, microphone and plenum transducer signals were also collected simultaneously.

The success of a Rayleigh scattering system depends on the use of clean, particle-free air, minimization of stray scattered light and providing a stable, vibration-free environment for some optical components. The last requirement is not as critical as for velocity and temperature measurements (where a Fabry–Perot interferometer is used). Since the facility was built to measure velocity and temperature, in addition to air density, special arrangements to minimize the effect of loud jet noise were discussed in Panda & Seasholtz (1999*a*). The primary jet was supplied with unheated, compressed air filtered to remove all dust particles. A clean co-flow through a coaxial nozzle of 200 mm diameter surrounded the primary jet. An external air filter and air handling

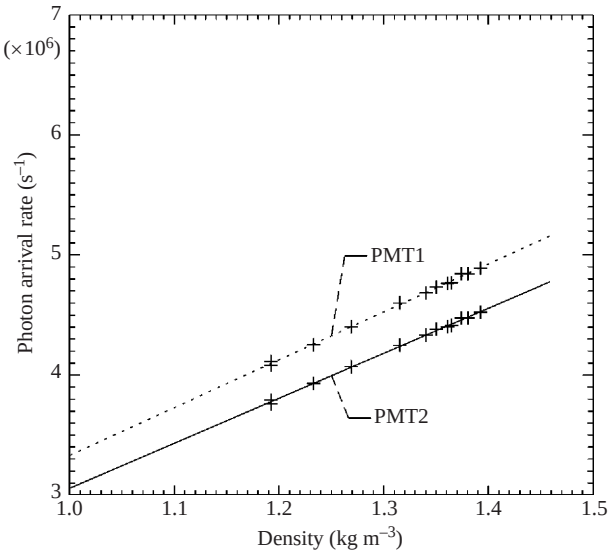

FIGURE 3. Calibration curves of Rayleigh scattered light to measure air density. Straight lines show least-square fit.

system were installed to produce this co-flow. The coaxial flow ensured dust-free air for the entrained flow. However a few particles were unavoidable. The second problem was stray reflected laser light. Due to the special orthogonal arrangement of the optical set-up, the primary laser beam intersected the nozzle block when the probe volume was close to the nozzle exit. Between the nozzle exit and 1.3 diameters downstream of the exit the stray background light overwhelmed the Rayleigh signature and no measurement was possible. The third problem was condensation during the operation of the Mach 1.8 nozzle. The primary supply air was dried to a dew point of -50° Celsius and moisture condensation was absent in the primary air jet. However, the entrained room air contained a significant amount of moisture, which condensed in the shear layer and caused significant stray scattering. An effective solution was found in operating the Mach 1.8 jet for a couple of hours continuously before starting the data acquisition. The jet facility was located in a closed test cell and a couple of hours of operation purged the moist room air and significantly reduced condensation.

2.2. *Density calibration*

A calibration process was necessary to determine the proportionality constant between the photon count rate and the air density, as well as to determine the residual stray light collected through the optics. The calibration was performed in the unheated plume of a convergent nozzle operated in the Mach number range of 0 to 0.99. At each operating condition the photon arrival rate was counted over a one second duration and the jet density is calculated using isentropic relations. Subsequently, a straight line was fitted through the data to determine the proportionality constants a and b:

$$N = (a\rho + b)\Delta t. \tag{4}$$

The additional constant b is needed to account for the room light and stray scattered laser light. Figure 3 shows sample calibration curves. Since two counters were used, two sets of calibration constants a_1, b_1 and a_2, b_2 were calculated. The calibration was

performed over a density range smaller than that encountered in the jet plumes. This is not of concern since the fundamental linear relationship between the molecular number density and intensity of scattered light holds true at any gas density.

2.3. *Time-average density and root-mean-square density fluctuation measurement*

The instantaneous flow density ρ is divided into a time-averaged part $\bar{\rho}$, and a fluctuating part ρ':

$$\rho = \bar{\rho} + \rho'. \tag{5}$$

Photoelectron counting ($N_i, i = 0, 1, 2, \ldots, n-1$) over a large number ($n = 65\,536$) of contiguous time bins covering more than 1 s time duration was used to measure the two parts. The mean density was related to the average of all bins N_{av}:

$$\bar{\rho} = \frac{1}{a}\left(\frac{N_{av}}{\Delta t} - b\right), \quad \text{where} \quad N_{av} = \frac{\sum N_i}{n}. \tag{6}$$

All density statistics presented here had to deal with the electronic shot noise arriving from the photomultiplier tube. (There should be no confusion between 'jet noise' and 'shot noise'; the former is an acoustic phenomenon while the later is photo-electronic in nature. Any optical intensity measurement is inherently affected by shot noise). Even when the incident light is of constant intensity (no density fluctuation), the rate of photoelectron emission by a PMT shows significant variation, referred to as statistical photon count noise or 'shot noise'. This noise is random in nature and follows Poisson's statistics. The density fluctuations cause the collected light intensity to vary and the joint statistics can be expressed through Mandel's formula (Saleh & Teich 1991). An important result of Mandel's formula is that the variance of the photon count σ_N^2 is a sum of the variance of shot noise, σ_{sh}^2, and the variance of the light power fluctuation, σ_P^2:

$$\sigma_N^2 = \sigma_{sh}^2 + \sigma_P^2. \tag{7}$$

The variance of photon count in time interval Δt was calculated from the measured data as

$$\sigma_N^2 = \sum_{i=1}^{n} \frac{(N_i - N_{av})^2}{N_i - 1}. \tag{8}$$

Another important result of Poisson's statistics is that the variance of shot noise is equal to the time average of all counts:

$$\sigma_{sh}^2 = N_{av}. \tag{9}$$

This allows the light power fluctuation measurement: $\sigma_P^2 = \sigma_N^2 - N_{av}$. It is straightforward to show that the equivalent variance in the density fluctuation, $\overline{\rho'^2}$, can be determined through the calibration constant a, and the time width Δt, of the individual bins:

$$\overline{\rho'^2} = \frac{\sigma_P^2}{a^2 \Delta t^2}. \tag{10}$$

The root-mean-square density fluctuation, ρ_{rms} was calculated as

$$\rho_{rms} = \sqrt{\overline{\rho'^2}}. \tag{11}$$

To reiterate, photon counting was performed over 65 536 time bins. The average (equation (6)) and mean square (equation (8)) were calculated; the former was subtracted

from the later; the mean-square fluctuation was determined through equation (10), and finally a square root of the mean square provides the r.m.s. density fluctuation.

The fundamental source of error in the time-averaged density data is once again from the shot noise. The relative uncertainty in the measurement of N is determined through equation (9) as

$$\frac{\sigma_{sh}}{N_{av}} = N_{av}^{-1/2}. \tag{12}$$

For the present experiment the count rate was high: between 5 and 8 million per second. Due to the small time width, the count accumulated in the individual bins was small, yet averaging over the large number of bins reduced the uncertainty to $< 0.05\%$. Since the contribution to uncertainty from the fundamental noise source was very low, that from a host of secondary sources became prominent. Occasional particles were unavoidable and their passage led to an increase in the count from the corresponding time interval. There were also very fine oil droplets, perhaps picked up from the air compressor, that caused a small difference in scattering intensity between the supply air and the cleaned ambient air. Although these secondary noise sources are difficult to quantify, the absolute density numbers are found to be repeatable within $\pm 1\%$ of their quoted values.

The primary error source in r.m.s. data was due to a small deviation from Poisson's statistics (equation (9)) in the PMT and photon-counting electronics. Data obtained from a quiescent clean air condition (steady light intensity) show that the average count deviated slightly ($\pm 2\%$) from the mean-square calculation. Since the difference between the mean square and mean count was used to calculate the root-mean-square density fluctuation, the above deviation produced a positive bias error of about 4%. The r.m.s. fluctuation measurement is susceptible to unsteadiness in the laser intensity, which fortunately was very small. The second major source of error was due to the passage of occasional particles through the probe volume. As the probe volume was moved from close to the nozzle exit to 14 diameters downstream, the number of particles increased progressively from a few per second to the order of 100 per second. Large particles passing through the probe volume were easily detected by examining the bin-to-bin variation, and removed by neglecting counts above 5 times the r.m.s. value. This procedure, however, could not account for the small increases caused by particles passing through the vicinity of the beam waist. The bias error increased progressively from the nozzle exit to farther downstream as a larger number of particles were entrained into the jet. No data were taken beyond a downstream distance of $15D$.

2.4. *Measurement of density fluctuation spectra*

The straightforward route to measure density fluctuation spectra is to calculate a discrete, one-sided spectrum from the sequence of photoelectron counts and multiply the power spectral density by appropriate calibration constants. The average value needs to be subtracted from the individual count, $N_i' = N_i - N_{av} (i = 0, 1, 2, \ldots, n-1)$, before the power spectrum is calculated:

$$P_{N'^2}(f_l) = \frac{2}{n^2} |F_{N'}(l)|^2, \quad f_l = \frac{l}{n\Delta t}, \quad l = 0, 1, 2, \ldots, \tfrac{1}{2}n - 1, \tag{13}$$

where

$$F_{N'}(l) = \sum_{i=0}^{n-1} N_i' \exp\left(j \frac{2\pi i l}{n}\right).$$

The power spectral density of the air density fluctuations becomes

$$P_{\rho'^2}(f_l) = \frac{1}{a^2 \Delta t^2} P_{N'^2}(f_l). \tag{14}$$

The problem with this straightforward method is that the calculated spectrum becomes overwhelmed by the electronic shot noise contribution. Following Parseval's identity and equation (8)

$$\sum_{l=0}^{\frac{1}{2}n-1} P_{N'^2}(f_l) = \sigma_N^2 = \sigma_{sh}^2 + \sigma_P^2. \tag{15}$$

In other words, the resultant spectrum is a sum of shot noise and the desired air density fluctuations. An estimate of the shot noise contribution can be obtained by noting that it is white noise and contributes nominally equally to all frequency bins f_l. Since $\sigma_{sh}^2 = N_{av}$

$$\text{Shot noise floor} = \frac{N_{av}}{\frac{1}{2}n}, \tag{16}$$

that is, the average value of all photoelectron counts divided equally among the number of frequency bins in the spectrum. A sample spectrum obtained through this process is shown later in this paper in figure 8. In general, the method was found to provide a crude estimate at the energetic low-frequency part, and was unable to resolve the high-frequency part of the spectrum. Shot noise contributes a fixed floor and a superimposed randomness to the spectrum. The latter could not be removed through the subtraction process.

In the improved technique the collected light was split into two nearly equal parts and measured with two PMTs. The simultaneous photoelectron counting produced two series of data N_{1i} and N_{2i} ($i = 0, 1, 2, \ldots, n-1$). The average values from each of the time series were subtracted: $N'_{1i} = N_{1i} - N_{1av}$, $N'_{2i} = N_{2i} - N_{2av}$, and a cross-spectral density

$$|P_{N'_1 N'_2}(f_l)| = \frac{2}{n^2} |F_{N'_1}(l) F^*_{N'_2}(l)| \tag{17}$$

significantly reduced the shot noise contribution. Superscript * in the above equation indicates complex conjugate. The density fluctuation spectra is calculated using appropriate calibration constants a_1 and a_2 for the two photomultiplier tubes:

$$P_{\rho'^2}(f_l) = \frac{|P_{N'_1 N'_2}(f_l)|}{a_1 a_2 (\Delta t)^2}. \tag{18}$$

Usually two long records, each of either 262 144 (for higher Mach number jets) or 524 288 (low Mach number jets) data points, were collected from multiple segments of 16 384 data strings. The latter is the maximum number of contiguous counts delivered by the photon counters. The Welch (1967) method of modified periodograms was used to calculate the cross-spectral density. Each long record was divided into small segments of 512 data points. The adjacent segments were overlapped by 50%. The modified periodograms of corresponding segments from the two PMTs were calculated and then used to determine local estimates of cross-spectral density. All local estimates were averaged to obtain the final cross-spectral density.

A source of experimental uncertainty in the spectral data is due to aliasing from the unresolved part of the fluctuation spectrum. The photon counting process does not allow for an external anti-aliasing filter as used in traditional signal processing. However, the counting process sums all fluctuations over the bin duration and acts

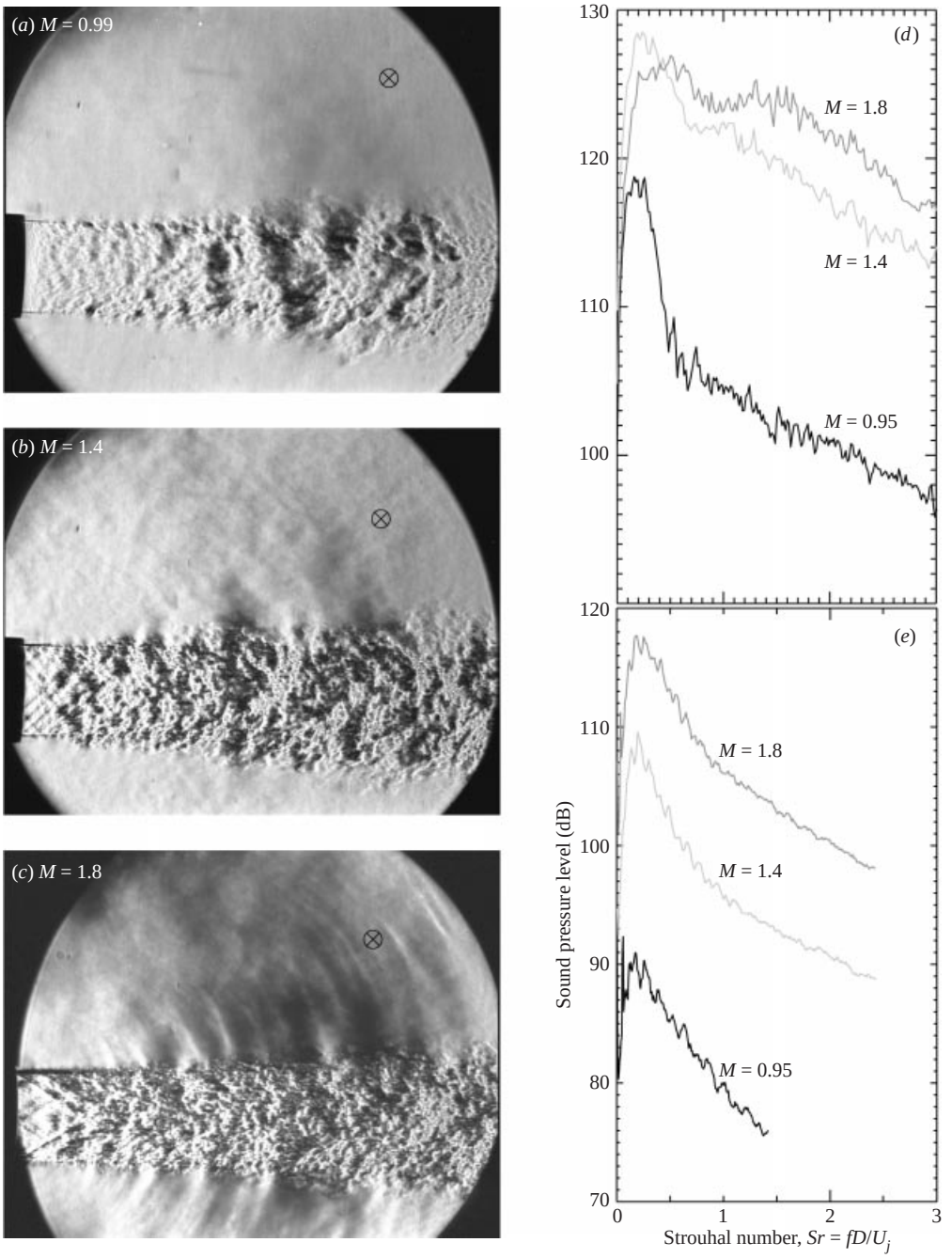

FIGURE 4. (*a–c*) Spark schlieren photograph of fully expanded jets at the indicated Mach number conditions; (*d*) pressure fluctuation measured at $x/D = 4$, $y/D = 2$ (shown by ⊗ in the schlieren photos); (*e*) sound pressure fluctuations at $50D$ and 30° to the flow direction.

as a special type of integrate-and-dump filter. A discussion of the filter response function is provided in the Appendix. To illustrate, a 10 ms bin width effectively yields a sampling rate of 100 kHz and the spectral information is resolved up to 50 kHz (sampling criterion). Figure 21, in the Appendix, shows that the sine-function filter response provides some low-pass filtering, but still a small part of the fluctuations occurring above the Nyquest frequency is expected to be folded back into the resolved range. Since energy associated with the high-frequency turbulence fluctuations is small to begin with, the aliasing error is expected to be small.

2.5. *Measurement of flow–sound cross-correlation*

A $\frac{1}{4}$ in. diameter microphone was kept at a fixed position in the far field and the laser probe volume was moved from point to point in the flow to determine the correlation between the flow density fluctuations and sound pressure fluctuations. The microphone was kept at either 30° or 90° to the flow direction (figure 1) and at a radius of 50 nozzle exit diameters. The microphone signal and the Rayleigh scattered light were measured simultaneously using, respectively, an analog-to-digital (A/D) converter and the photon counting electronics. An external timer signal was used to synchronize the acquisition processes. The timer signal was obtained from a signal generator, programmed to produce a square wave of desired time period. The A/D conversion occurred at each rising edge of the square wave, which also marked the beginning of individual time bins for photon counting. A time bin ended at the following rising edge.

To verify time synchronization of the entire acquisition process, a synthetic signal was measured and compared. The synthetic signal (which was a square wave from a separate generator) was used to drive an electrostatic actuator as well as a photo-diode. The electrostatic actuator provided excitation at a synthetic signal frequency to the microphone diaphragm. The photo-diode produced light intensity modulation at the synthetic signal frequency. The photo-diode was placed in front of the collection fibre so that the photomultiplier tubes received the modulated light. Finally, the above data acquisition electronics were used to collect microphone and photo-diode signals. Satisfactory synchronization, observed over all frequency ranges tested, provided confidence in the acquisition process.

The microphone was calibrated using a Pistonphone and the calibration constants were used to convert the voltage signal to instantaneous sound pressure fluctuation p'. The cross-correlation-density function between air density and sound pressure fluctuations was calculated using the sequence of photon counts N'_{1i} and digitized microphone signal p'_i:

$$P_{N'_1p'}(f_l) = \frac{2}{n^2}(F_{N'_1}(f_l)F^*_{p'}(f_l)), \quad P_{\rho'p'}(f_l) = \frac{P_{N'_1p'}(f_l)}{a\Delta t}. \tag{19}$$

The cross-spectral density has real and imaginary parts,

$$P_{\rho'p'}(f_l) = \mathrm{Re}\, P_{\rho'p'}(f_l) - \mathrm{iIm}\, P_{\rho'p'}(f_l), \tag{20}$$

which are used to determine the magnitude and coherence function:

$$\left.\begin{aligned} |P_{\rho'p'}(f_l)| &= \sqrt{\mathrm{Re}^2 P_{\rho'p'}(f_l) + \mathrm{Im}^2 P_{\rho'p'}(f_l)}, \\ \Gamma^2_{\rho'p'}(f_l) &= \frac{|P_{N'_1p'}(f_l)|^2}{P_{N'_1N'_1}P_{p'p'}(f_l)} \end{aligned}\right\} \tag{21}$$

Since the collected light was split and measured with two counters, the cross-

correlation was performed twice: between microphone signal and either one of the two series of counts. Finally, an average of the two results was calculated. The cross-correlation minimizes shot noise in the photon count data, but a noise floor persists. To lower the noise floor, more than half a million (524 288) data points were collected for each data string. The Fourier transform used the segmenting and averaging process as outlined in the previous subsection.

An important issue of propagation delay had to be considered in the cross-correlation and cross-spectral density calculations. The sound waves radiated from the flow fluctuations require finite time (distance of microphone/sound speed) to reach the far-field microphone. Therefore, the time signature of the 'effect' (sound pressure fluctuation) is expected to lag behind the time signature of 'cause' (turbulent fluctuations). Unlike the calculations for density spectra, longer segments of the data string (4096) were used to account for this propagation time delay. From a consideration of the sampling rate and microphone distance it was determined that for the present case only the first few (at most 8%) data strings were affected by the time delay. By changing the length of data strings it was confirmed that segments of 4096 data provided satisfactory convergence of cross-spectral density value.

3. Results and discussion

The choice of the three Mach number conditions (0.95, 1.4 and 1.8) was deliberate. The purpose was to cover a range where both subsonic and Mach wave radiation mechanisms produce jet noise. The schlieren photographs and the microphone spectra presented in figure 4 show that this goal has been attained. (In figure 4*a* one previously obtained schlieren photograph for the Mach 0.99 jet is used.) It is known that in a supersonic jet, when turbulent eddies attain a speed faster than the ambient sound speed, a Mach wave emission process begins (Lowson & Ollerhead 1968; Bishop, Ffowcs Williams & Smith 1971; Papamoschou 1997). The Mach waves are ballistic shock waves attached to the supersonic eddies. The differences in the schlieren photographs for the three jets are primarily due to the inception of the Mach wave emission process. Traces of these waves are visible in the photograph for the Mach 1.4 jet, while a stronger radiation pattern is visible in at Mach 1.8. There is a wide spread, between $0.89U_j$ to $0.6U_j$, where U_j is the jet centreline velocity, in the convective velocity of turbulent eddies reported by various researchers. The estimated convective velocity (table 1) is always subsonic with respect to the ambient sound speed for the Mach 0.95 jet; the Mach 1.4 jet is at the borderline, while eddies in the Mach 1.8 jet are expected to attain supersonic speed. To determine the frequency of emission a microphone was kept in the near field at the position marked by $\otimes$ in the schlieren photographs. The respective microphone spectra are shown in figure 4(*d*). These spectra confirm Mach wave radiation for the Mach 1.4 and 1.8 jets and their absence in the Mach 0.95 jet. There is a common sharp hump at a lower Strouhal number ($Sr = fD/U_j, f$ being frequency in Hz and D nozzle exit diameter) around 0.2 in the near-field spectra of figure 4(*d*). The hump is associated with large vortices present at the end of jet core. Zaman (1986) reported that the footprints of the vortices are seen along the entrained flow streamlines. Mach wave emission dominated the high-frequency part of the sound spectra and peaked around $Sr = 1.5$. The far-field sound pressure spectra are presented in figure 4(*e*). The 30° angle was chosen to coincide with the peak sound radiation direction for cold jets as reported by Yu & Dosanjh (1972). It should be pointed out that the ripples superimposed on the microphone spectra are telltale signs of reflection caused by large optical components

Nozzle type	Convergent operated at $M = 0.95$	C–D $M = 1.4$	C–D $M = 1.8$
Minimum shock operation M	–	1.395	1.795
Reynolds number Re_D	0.66×10^6	1.16×10^6	1.88×10^6
Jet velocity U_j ($m\,s^{-1}$)	316	411	486
Estimated eddy convection speed U_c ($m\,s^{-1}$) $= 0.6U_j$–$0.89U_j$	190–282	247–366	292–433
Jet density ρ_j ($kg\,m^{-3}$)	1.36	1.6	1.89
Difference ($\rho_j - \rho_a$) ($kg\,m^{-3}$)	0.2	0.44	0.73
Frequency (kHz) for $Sr = 1$	12.4	16.2	19.1

TABLE 1. Operating conditons: specific heat ratio, $\gamma = 1.4$; total temperature, $T_0 = 300\,K$; ambient density, $\rho_a = 1.16\,kg\,m^{-3}$, ambient sound speed, $a = 347\,m\,s^{-1}$. C–D denotes converging–diverging.

placed around the jet. Nevertheless, the primary difference in spectra between the subsonic and supersonic conditions is seen as an increase in the overall level and a more energetic high-frequency part. In a nutshell, figure 4 demonstrates that the three Mach number jets used in this experiment covered both subsonic and Mach wave sound emission regimes.

At this point it is worth differentiating two types of 'Mach wave' radiation processes described in the current literature. The original description (Lowson & Ollerhead 1968; Bishop *et al.* 1971; Ffowcs Williams 1963), as outlined above, applies to supersonically convected eddies. Chronologically, the earlier works are based on the view that turbulence is made up of small random eddies. The advent of a newer view, that a significant part of the jet turbulence is made up of hydrodynamic instability waves with long coherence length, brought a different description of Mach wave emission. The work of Tam & Burton (1984) and Morris & Tam (1979) established that at any convection velocity hydrodynamic instability waves, subjected to amplitude modulation (associated with the growth and decay), are capable of radiating sound by Mach wave emission. This new description is explained in wavenumber space. A given frequency ω and wavenumber α instability wave is, due to the amplitude modulation, capable of producing sound at a small wavenumber α_s such that $\omega/\alpha_s \geqslant a_0$ (ambient sound speed). Schlieren photographs, similar to figure 4, validate the presence of Mach waves at supersonic convection speed. However, Mach wave generation by instability waves at subsonic convection speed cannot be verified.

As a prelude to density data, some important aspects of viewing a jet flow through this parameter should be discussed. In a low-speed unheated air jet, the density variations are negligibly small. As the jet velocity is increased (or if the jet is heated), the density difference between the ambient air and the jet core increases. For the present unheated case, increasing Mach number caused an increase in cooling which, in turn, increased the density of the primary air jet. The turbulent density fluctuations are caused by simple mixing between the ambient and primary jet fluid, as well as by the inertial effects (local acceleration and deceleration) of flow. The former perhaps contributes more to the density fluctuations, although the inertial effects are expected to be the source of acoustic radiation. Table 1 shows the density difference in the present experimental conditions. The accuracy of the present technique to measure density fluctuations improves as the density difference increases. Therefore, measurements made from higher Mach number conditions are expected to be more accurate. The experimental data are non-dimensionalized by the difference between the jet

centreline and the ambient density ($\rho_j - \rho_a$). The time-averaged data ($\bar{\rho}$) were non-dimensionalized as $(\bar{\rho} - \rho_a)/(\rho_j - \rho_a)$. Here ρ_j is the jet core density calculated from isentropic relations and ρ_a is the ambient density. The parameter is unity at the core and drops to zero as the ambient condition is reached. The fluctuating density data were also normalized by $(\rho_j - \rho_a)$, i.e. $\rho_{rms}/(\rho_j - \rho_a)$. A minor disadvantage of this normalization is that the uncertainty in the data finally presented increases with a decrease of the jet Mach number. The same uncertainty of $\pm 1\%$ in the absolute measurement of time-averaged density is manifested as an error of $\pm 5\%$ in the non-dimensionalized presentation of data from the Mach 0.95 jet and of $\pm 1.5\%$ for the Mach 1.8 jet.

3.1. *Time-averaged data*

The centreline variation is shown in figure 5. The converging–diverging nozzle measurements were performed at a pressure ratio that produced the weakest shocks in the core. Note that a completely shock-free plume is never realized from the C–D nozzles at supersonic operating conditions. A literature survey of earlier data confirms this observation. Supersonic jets are wave-guides and a small manufacturing irregularity or even the shear layer turbulent fluctuations will produce standing waves in the form of weak shocks. The least-shock-operation point was determined by changing the operating pressure ratio and by measuring the shock strength. For the present nozzles the least-shock operation was measured to be at $M = 1.395$ and 1.795, which were close to the design conditions of $M = 1.4$ and 1.8.

Traditionally, the flow quality from a converging–diverging nozzle is judged from the centreline total pressure surveys using Pitot tubes. The majority of flow data available in the literature were obtained using a Pitot tube. Figure 5(*a*) shows results obtained from such measurements made in the present nozzles. Following conventional practice, the measured total pressure is converted into Mach number using Rayleigh's equation, assuming static pressure inside the jet is equal to the ambient pressure (Liepmann & Roshko 1958). Clearly, the periodic undulations visible in the Rayleigh data are almost absent in the Pitot tube data, which in fact provides the impression that the nozzles are operating nearly shock free! The Pitot tube measures total pressure, which hardly varies across a weak shock and, therefore, the inferred Mach number value hardly shows any change. Density, on the other hand can show significant variation. The centreline surveys of figure 5(*b*) show that the undulations from a weak shock pattern persist far beyond the potential core. The spatial distance between the peaks and valleys reduces progressively, perhaps as a result of the reducing local Mach number. The inset schlieren photographs confirm the presence of the weak shocks. Downstream from the nozzle exit the spatial distance between the peaks and valleys reduces progressively, perhaps as a result of the reduction in local Mach number. For the present unheated jet, centreline density decays to the lower ambient value. Jiang & Sislian (1998) used Rayleigh scattering to measure centreline decay of heated jets where density increased to the ambient value.

The root-mean-square density fluctuations of figure 5(*c*) shows that the turbulent fluctuations remain low in the potential core, then start to grow at a fast rate, and finally taper off slowly. As the potential core becomes longer with an increase of Mach number, the peak positions of the r.m.s. density fluctuation also move further downstream. The peak fluctuations are about $0.22(\rho_j - \rho_a)$. The relative uncertainty level in the fluctuation data is higher due to the shot noise subtraction process described earlier. In addition to a 4% bias error, there is a random uncertainty of $\pm 4\%$. As mentioned earlier, the number of particles passing through the probe volume increased progressively and particularly affected data points obtained beyond

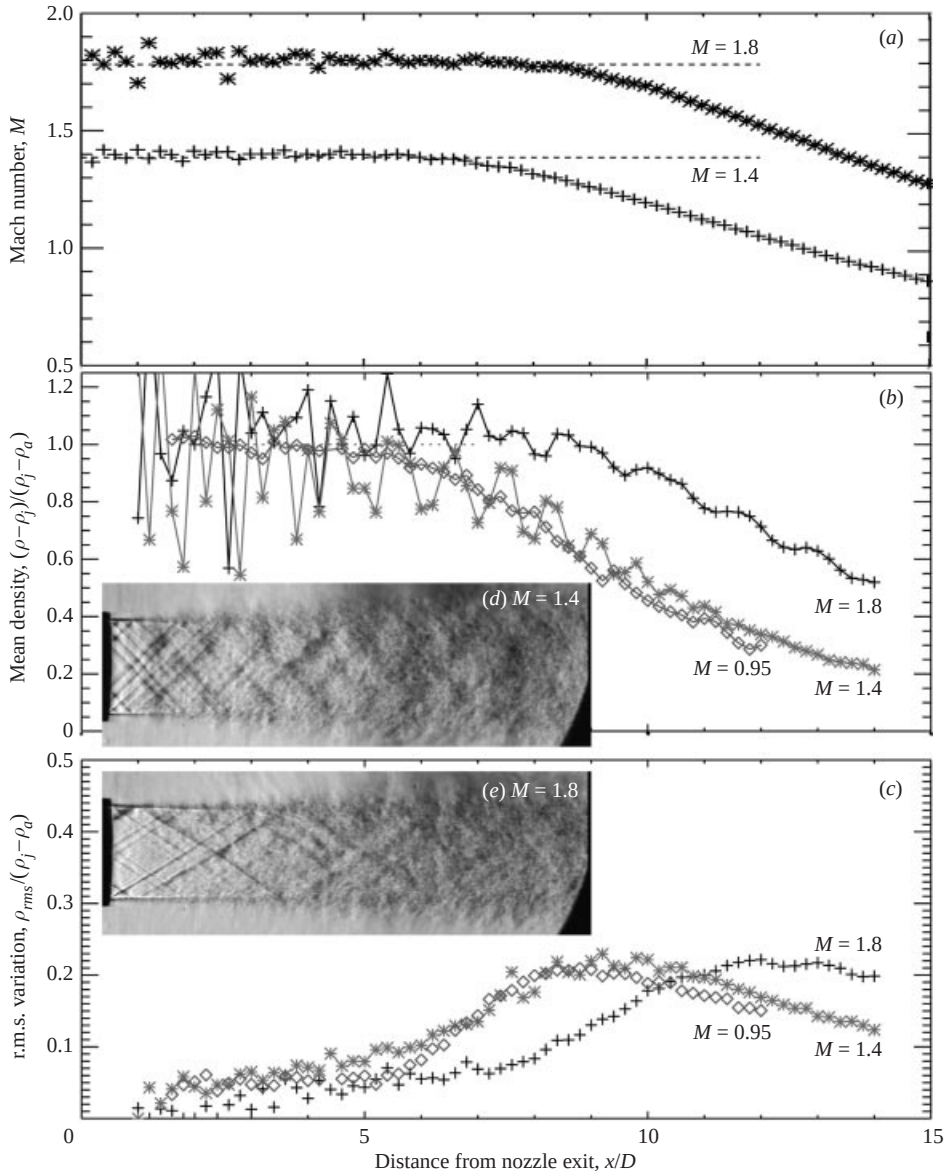

FIGURE 5. Centreline variations of (*a*) time-averaged Mach number measured by a Pitot tube, (*b*) time-averaged density and (*c*) root-mean-square density fluctuations for Mach number jets as indicated. The insets (*d*) and (*e*) are time-averaged schlieren photographs.

the potential core. The measured data from this region are expected to be biased towards even higher values. The r.m.s. density fluctuations can be nearly zero under two situations: first, if the turbulence fluctuations are very low, as in the potential core of the jet; and second if the flow velocity decays to the incompressible regime, such as in the far field of jet development. In the second situation, there would be significant velocity fluctuations while density fluctuations would be insignificant.

The jet spreading, due to the growth of the shear layer, is shown in the time-averaged radial surveys of figure 6. The corresponding time-averaged velocity and

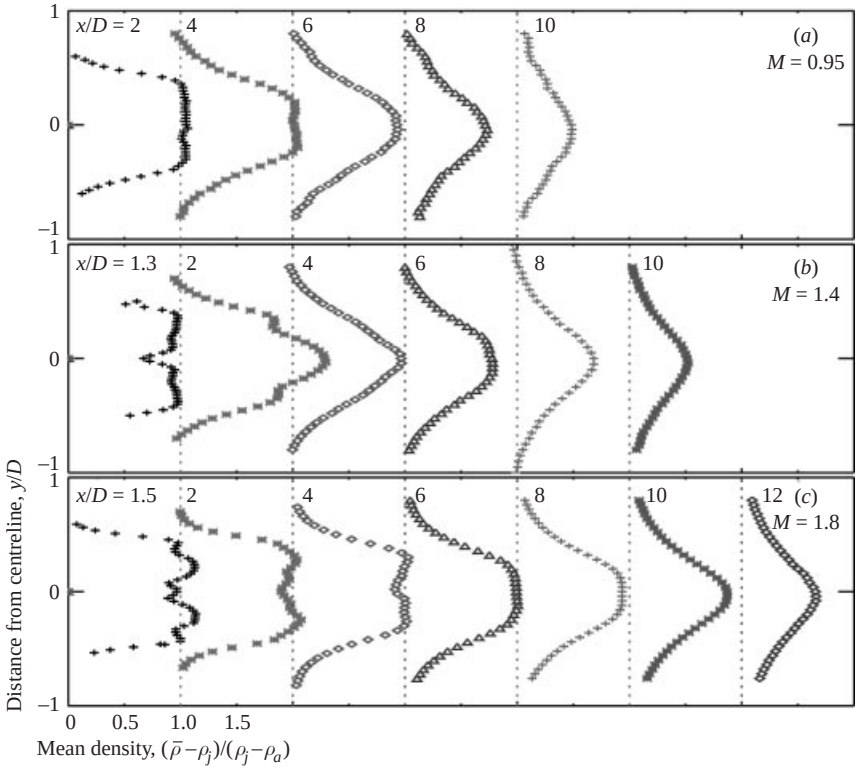

FIGURE 6. Radial profiles of time-averaged density measured at the indicated axial stations and Mach number conditions.

temperature data, measured using a spectrally resolved Rayleigh scattering technique, can be found in Panda & Seasholtz (1999*a*). The radial profiles demonstrate a progressive growth of the shear layer. The higher Mach number, $M = 1.8$, jet has the expected trend of a slower spreading rate compared to the Mach 0.95 case. The deviations from a top-hat distribution, in the measured profiles from close to the nozzle exit, are due to the presence of the weak shock cells. The radial profiles of r.m.s. density fluctuation are shown figure 7. At the closest measurement station from the nozzle exit, the fluctuations peak in the shear layer around $y/D = \pm 0.45$. The fluctuation profile at $x/D = 2$ shows a fully turbulent shear layer with a quiescent core. The peak locations progressively approach the centreline. Beyond about $10D$ for the Mach 0.95 jet and $12D$ for Mach 1.8 jet, the centreline is the location for peak fluctuations. There is very little information on experimental measurement of scalar turbulent fluctuations in the available literature. One exception is the crossed-beam measurements of Wilson & Damkevala (1970). The cross-correlation between signals from two perpendicular, intersecting beams provided measurements of r.m.s. density fluctuations. In a Mach 0.6 jet they reported peak $\rho_{rms}/(\rho_j - \rho_a) \approx 0.2$, which agrees well with the present measured level.

By presuming that the ambient pressure is imposed everywhere in the jet plume (i.e. local pressure $p = p_{amb}$) it is possible to calculate time-averaged temperature from density. The inverse of the density profile becomes the temperature profile $\bar{T} = p_{amb}/(\bar{\rho}R)$, where R is the universal gas constant (Jiang & Sislian 1998). The above assumption may not be valid in a supersonic stream, where weak waves can

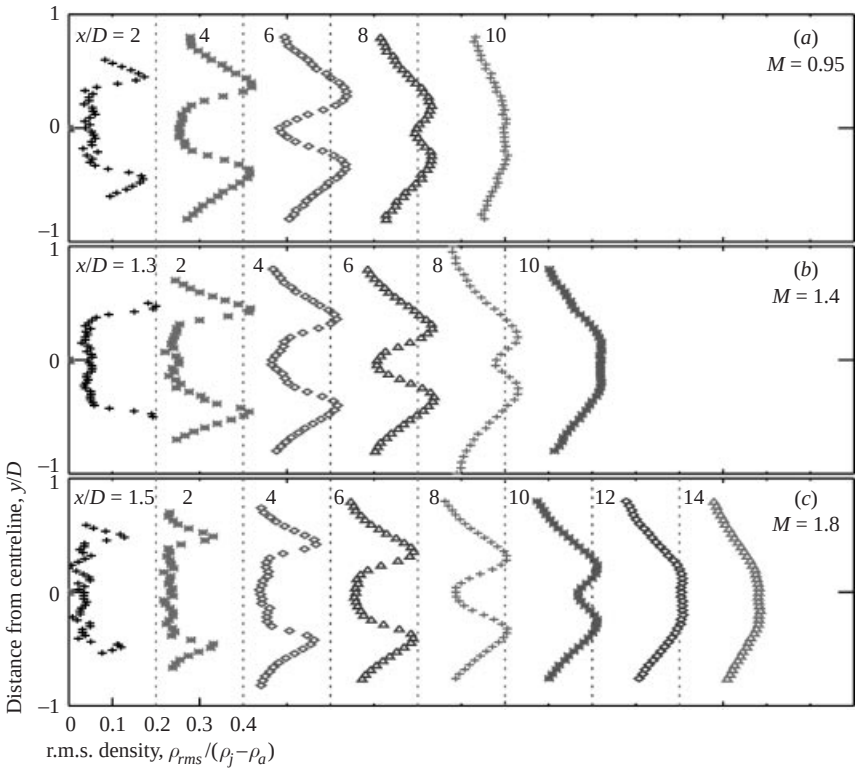

FIGURE 7. (*a–c*) Radial profiles of root-mean-square density fluctuations measured at the indicated axial stations and Mach number conditions.

produce pressure variation. It is also known that even in a subsonic jet local static pressure can deviate from the ambient pressure (Hussain & Clark 1977; Zaman 1986). Therefore, no attempt is made in the present paper to calculate local temperature.

3.2. *Density fluctuation spectra*

Figure 8 shows the outcome and improvements attained using two PMTs rather than a single PMT. As expected, the density fluctuation spectra from a single PMT signal are significantly affected by electronic shot noise. The dashed line shows the noise floor, obtained from (16). The cross-correlation between two PMT signals significantly reduces the shot noise contribution, enabling an improved definition of the spectral shape. The improvements are especially prominent at the high-frequency end. Neverthless, a complete elimination of shot noise is impossible to attain and as in any other spectral measurement a residual level persists. The finite number of data points used for the correlation and various electronic noise sources determine the residual level. An estimate of this residual level was obtained from data obtained at the 'no-flow' condition – the primary jet was turned off but the clean co-flow was present. Since there were no density fluctuations the spectral content was mostly due to the residual noise. The two-PMT technique was used for the no-flow spectra, a sample of which is also presented in figure 8. Note that the no-flow spectrum shows a ramp increase at the low-frequency end. This increase is associated with the passage of occasional dust particles through the probe volume (Seasholtz & Panda 1999). The data set for the no-flow spectrum was obtained 10 diameters away from the nozzle

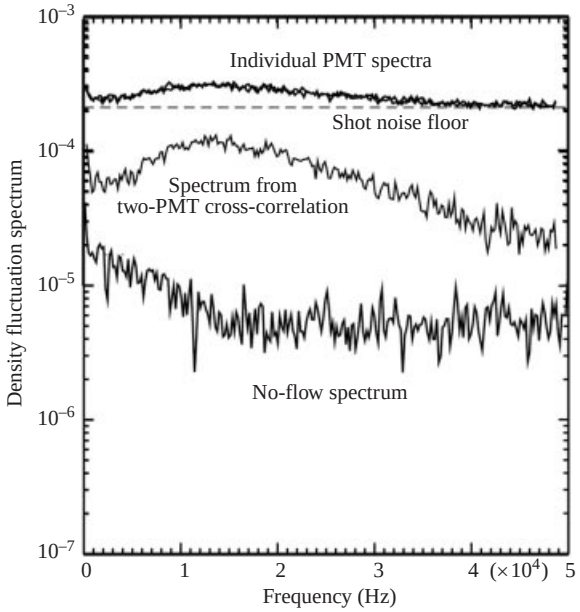

FIGURE 8. Improvement in the measurement of the density fluctuation spectrum using the two-PMT cross-correlation technique. Data for upper two curves from Mach 1.8 jet at $y/D = 0.48$ and $x/D = 2.4$. The no flow spectrum from the centreline and $x/D = 10$.

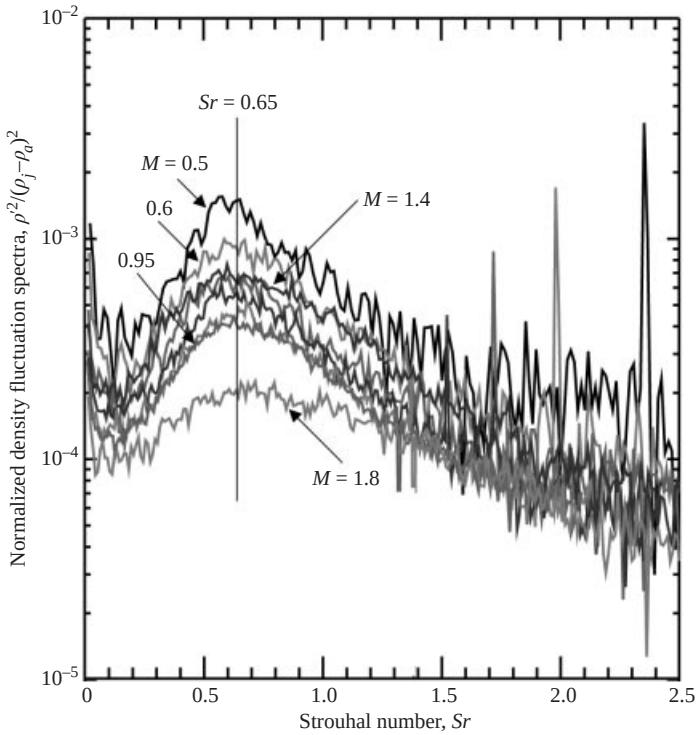

FIGURE 9. Density fluctuation spectra in $M = 0.5$, 0.6, 0.7, 0.8, 0.9, 0.95, 1.4 and 1.8 jets from a fixed point $x/D = 2.5$, $y/D = 0.45$ (0.48 for $M = 1.8$). The vertical line locates spectral peaks. Sharp spikes in some spectra are due to electronic noise.

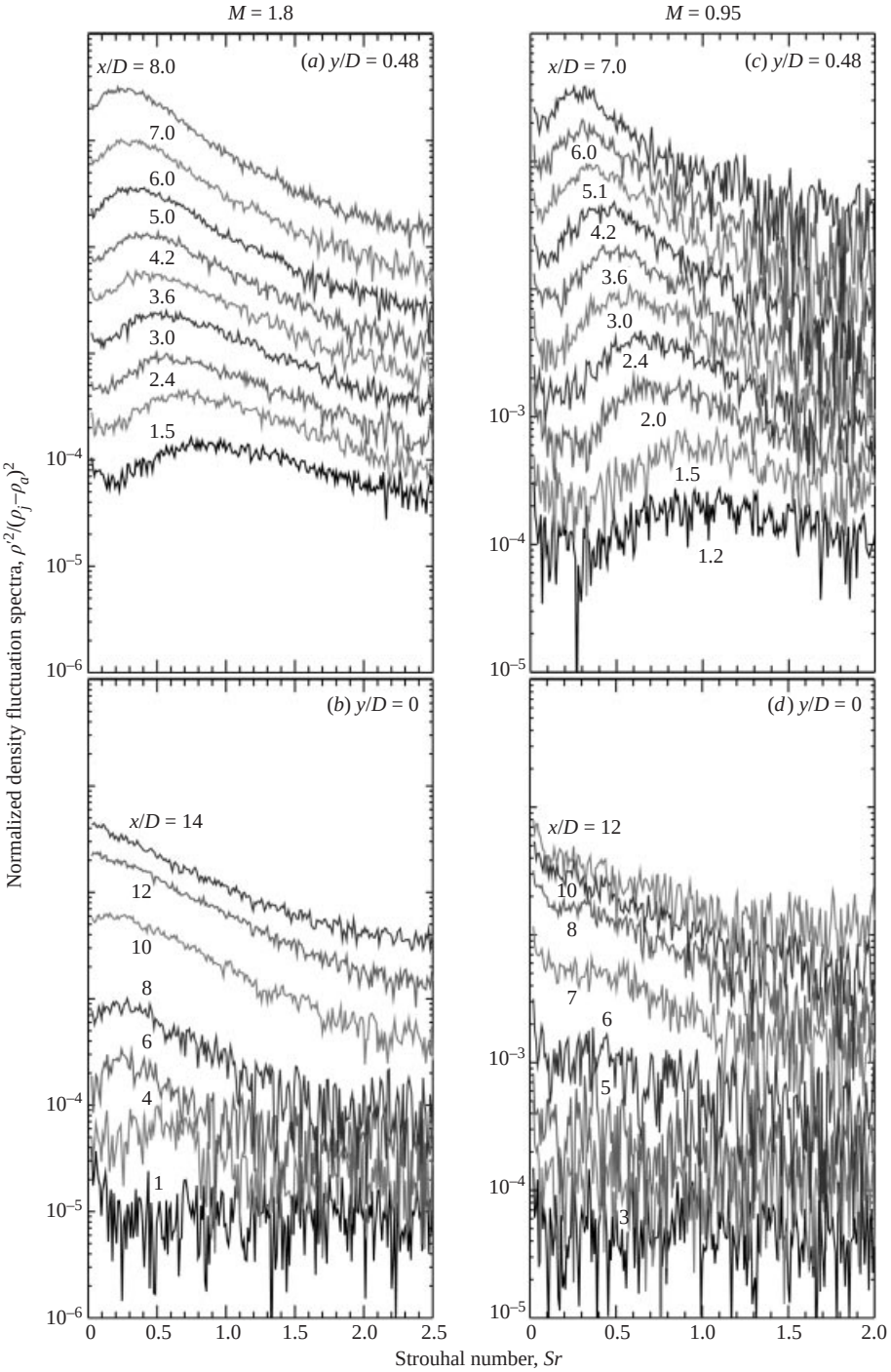

FIGURE 10. Density fluctuation spectra measured at the indicated axial stations and along (*a*), (*c*) $y/D = 0.48$ and (*b*), (*d*) the centreline of the Mach 0.95 and 1.8 jets. Individual spectra are separated by a multiplication factor of 2.

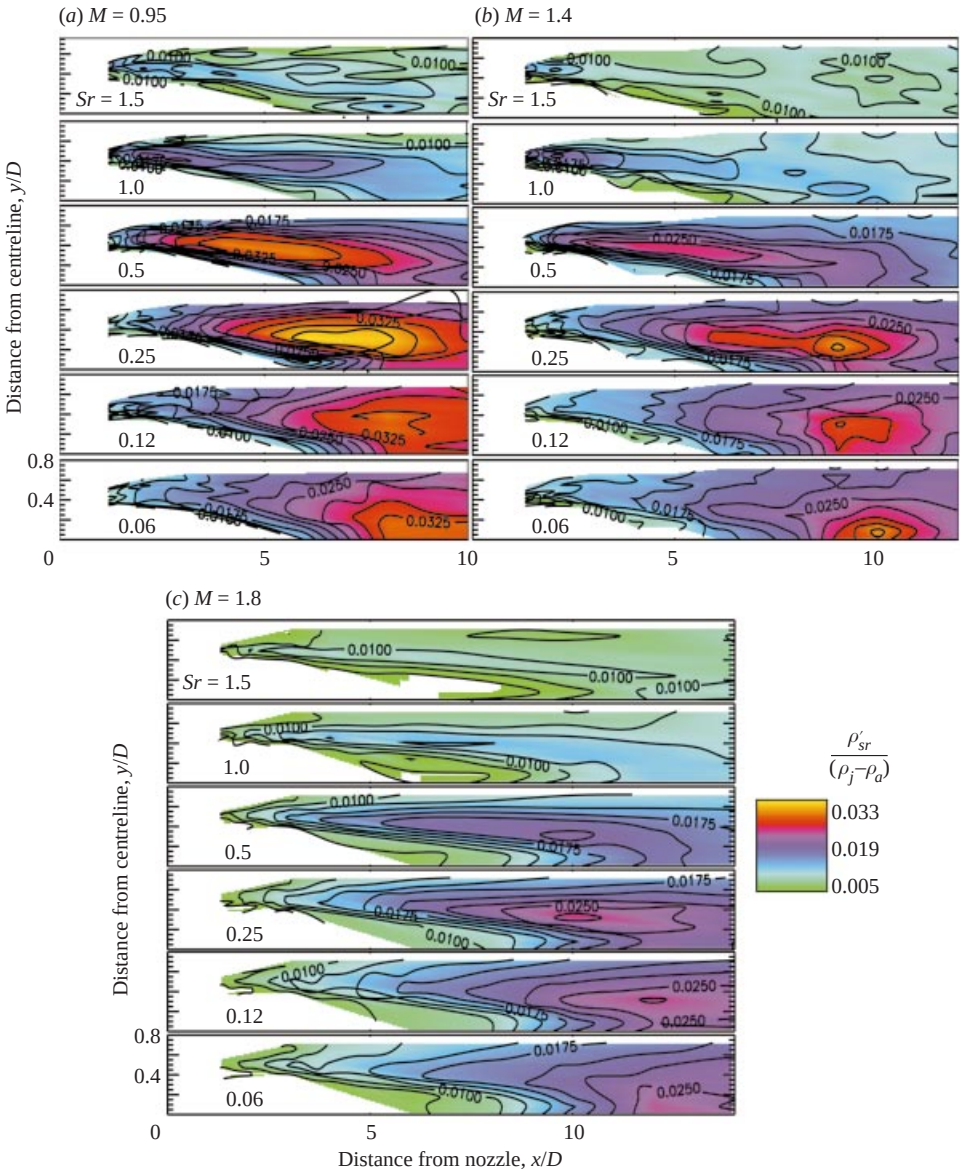

FIGURE 11. Distribution of density fluctuations at the indicated Strouhal frequencies for three different Mach numbers. Fluctuations were measured over 195 Hz band. Contours are at intervals of 0.0025.

exit where the particle entrainment rate was relatively high. Such spectra obtained close to the nozzle exit do not show the low-frequency contribution. Nevertheless, all density spectral descriptions should be compared with the no-flow baseline, with the part above the baseline being the desired spectrum. In addition to the noise base, the density spectra have a random uncertainty, the extent of which is visible in the randomness superimposed on the basic spectral shape.

The measurement technique was applied to determine the effect of the Mach number on density fluctuation spectra. For this purpose the laser probe volume was kept at a fixed position in the shear layer and the plume Mach number was varied in

the range $0.5 \leqslant M \leqslant 1.8$. The resultant spectra are shown in figure 9. When frequency values were normalized to the Strouhal number, and spectral density by $(\rho_j - \rho_a)^2$, an interesting fact emerged: the broadband peak was always found to occur around $Sr = 0.65$. The shapes of the individual spectra are also similar; the dissimilarity of the Mach 1.8 case is due to the slightly different radial location of the probe volume. Hot-wire measurements in low Mach number jets, $M < 0.5$, show a similar trend. The lowest Mach 0.5 spectra have some similarity with the pressure fluctuation spectra reported by Armstrong *et al.* (1977). The fact that this trend extends to supersonic conditions is experimentally verified for the first time.

Figure 10 presents a comparison between the density fluctuation spectra in the Mach 0.95 and 1.8 jets. Parts (*a*) and (*c*) were measured along the peripheral shear layer and parts (*b*) and (*d*) were along the centreline. The data from the shear layer show a gradual shift in the spectral peak from $Sr = 1.0$ to 0.2 with an increase in the downstream distance. The trend follows velocity fluctuation measurements in a low-speed jet (Crow & Champagne 1971) and expectations from hydrodynamic stability analysis. The latter establishes that an increase in shear layer thickness with downstream distance leads to increased amplification of progressively longer wavelength and lower frequency Kelvin–Helmholtz instability waves. The spectra measured along the centreline (figures 10*b* and 10*d*), however, differ from the velocity fluctuation measurements at low speed. Unlike the low-speed measurements there is no definite hump at the passage frequency of large organized structures. For the Mach 0.95 jet the peak values of all spectra appear at the lowest measured frequency. For the Mach 1.8 jet, weak humps are visible close to the nozzle exit, yet further downstream the peak occurs at the lowest measured frequency. The primary observation from figure 10, however, is the overall similarity in the spectral shapes, along both the centreline and the shear layer, between the two widely separated Mach number conditions.

This similarity is further explored in figure 11 where fluctuations occurring in the individual Strouhal frequencies are plotted from a large data set. The density fluctuation spectra were measured at a large number of points (8 to 12 axial by 10 radial points), and the mean-square fluctuations occurring at desired frequency bins were separated. For a uniform comparison, the square root of the mean-square fluctuations was non-dimensionalized by the difference of density between the jet core and the ambient density. In other words, from equation (18) the plotted variable can be written as

$$\frac{\rho'_{sr}}{\rho_j - \rho_a} = \frac{\sqrt{P_{\rho'^2}(f_0)}}{\rho_j - \rho_a}, \tag{22}$$

where the frequency bin f_0 corresponds to the desired Strouhal number. The process is the same as applied to the earlier root-mean-square data. Figure 11 shows similarity in the distribution of turbulent fluctuations in the three Mach number jets considered. Fluctuations at the highest Strouhal number occur close to the nozzle lip and in the shear layer. The position of the peak fluctuations progressively moves downstream as lower Sr are considered. $Sr = 0.25$ shows the highest fluctuation at the end of the potential core and at $y/D \approx 0.3$. The fluctuations occurring at even lower Strouhal number, e.g. $Sr = 0.06$, peak close to the centreline and further downstream. The primary change visible in the fluctuation pattern is an overall stretching with an increase in the Mach number. The slower growth of the instability waves and the resultant slower mixing process is the reason behind this stretching process. Returning to the sound pressure fluctuation data of figure 4, it is seen that the noise

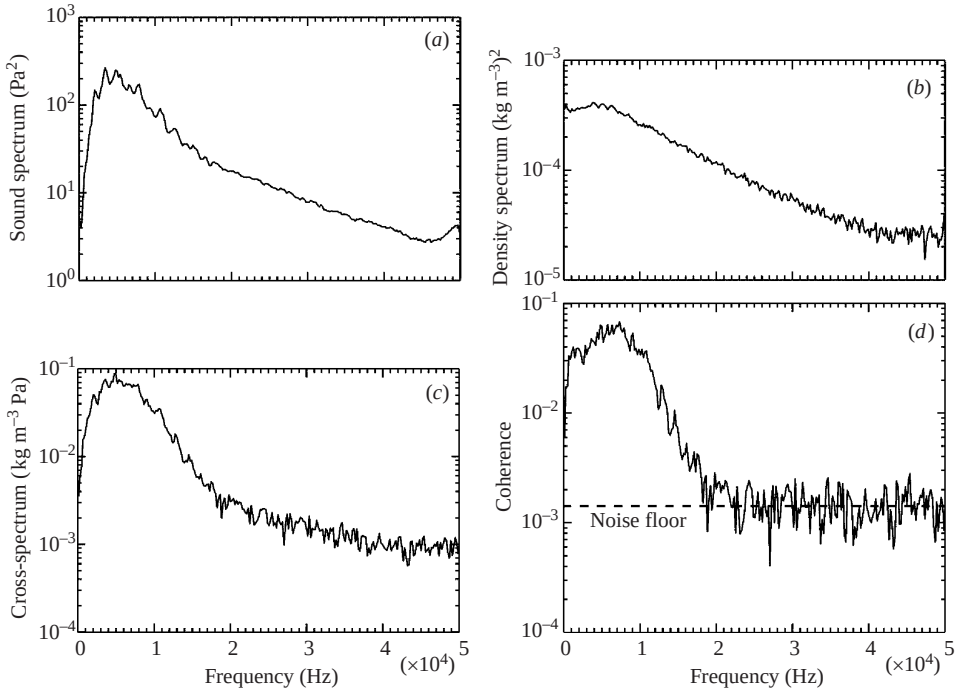

FIGURE 12. Cross-correlation (expressed as spectral density) between flow density fluctuations and sound pressure fluctuations in the Mach 1.8 jet; laser probe at the centreline and $x/D = 10$, microphone at the far field $r/D = 50$, $\theta = 30°$. (*a*) Sound pressure spectrum, (*b*) density spectrum, (*c*) cross-spectrum and (*d*) normalized cross-spectrum (coherence).

characteristics of the three Mach number jets are significantly different. This is in contrast with the similarity in the turbulent fluctuations. This led to the correlation measurement between the flow fluctuations to the far-field noise described in the next subsection.

3.3. *Flow–sound correlation*

The intermediate steps in the calculation of cross-spectral density between air density fluctuations and sound pressure fluctuations are illustrated in figure 12. Part (*a*) shows the sound pressure fluctuation spectrum in a dimensional form. Part (*b*) shows the density spectrum measured using two PMTs. Part (*c*) presents the magnitude of the cross-spectrum (first part of equation (21)). Finally, part (*d*) shows the coherence function obtained by normalizing the cross-spectrum by the microphone spectrum and the spectrum of a single PMT output. The shape of the coherence function in figure 12(*d*) is typical for measurements performed at the end of the potential core at most Mach number conditions. Note that the two-PMT correlation process, used for density fluctuation measurement, was not used for flow–sound correlation. Instead, the output from each PMT was separately correlated with the microphone signal and an average between the two results was finally presented.

The coherence function Γ provides a measure of the linear dependence between the flow fluctuations and the sound fluctuations. A coherence of unity implies a perfectly linear cause and effect relation while a value of zero implies no correlation. In reality, the zero coherence was never measured due to the presence of a basic noise floor. Before preceding further, an estimation of the noise floor in the calculations of

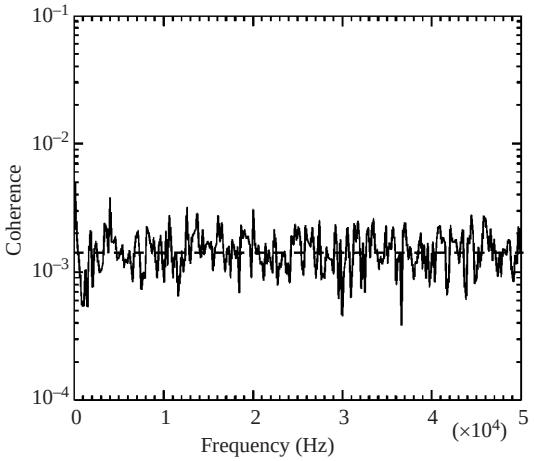

FIGURE 13. Normalized cross-spectrum between density and sound fluctuations at no-flow condition (jet turned off). Laser and microphone positions are as in figure 12. Dashed line represents the average noise floor.

the coherence function is necessary. Similar to the density fluctuation data, the cross-correlation data are affected by electronic shot noise. The shot noise is independent of the microphone signal; therefore, the cross-correlation process is expected to remove it. However, a residual floor was always retained. To estimate this level, the jet was turned off (keeping the co-flow on) and the coherence function between the microphone and the PMT signals was measured. Figure 13 shows the base noise level obtained from these no-flow data. The dashed line in figure 13 shows an average noise floor. In this paper, most of the plots of coherence functions are accompanied by a dashed line indicating average noise floor. For example, the dashed line in figure 12(d) shows that the coherence function measured beyond 20 kHz is completely due to the base noise lever ($\Gamma \approx 0.0015$). However, for fluctuations slower than 20 kHz, the measured coherence is significantly above the noise base. When measured coherence at a given frequency is above the noise floor, it can be said that some part of density fluctuation at that frequency from the laser probe location is creating sound pressure fluctuations at the microphone location; in other words, the probe location is a sound source.

An additional comment on the noise floor is that it is found to be nearly unchanging (varies between 0.001 and 0.002) at all Mach numbers down to the no-flow condition. This was confirmed by correlating density fluctuations in the potential core, close to the nozzle exit, at various Mach number conditions with a fixed far-field microphone. The noise floors apparent in many other coherence plots presented in the paper also support this observation. In order to check the effect of the number of averages on the noise floor, the cross-spectral density function of figure 13 was calculated using variable data length of 16k, 32k, 64k and 128k, keeping the segment length constant at 4096 samples. The exercise showed that the basic noise floor remained the same in all cases while the superimposed random uncertainty increased with a decrease in data length. The randomness superimposed on the basic shape represents convergence uncertainty in the coherence function calculation.

Since almost all of the earlier studies (Schaffer 1979; Lee & Ribner 1972 among others) presented data in terms of a simple correlation coefficient (time domain) instead of the cross-spectral density (frequency domain) used here, figure 14 was

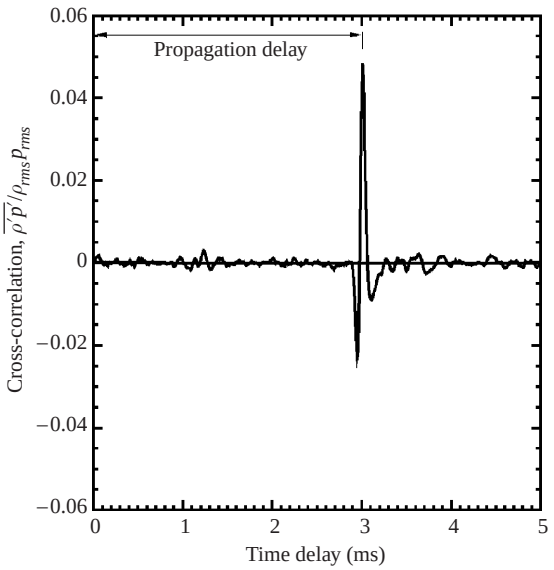

FIGURE 14. Cross-correlation from same data sets used in figure 12.

generated to bridge this gap. The same data sets used in figure 12 were reprocessed to obtain a cross-correlation in the time domain. The extra processing involves taking an inverse Fourier transform of the cross-spectral density function. The sharp spike in the correlation plot of figure 14 appears at a time delay that exactly corresponds to the time required for the sound waves to travel the distance between the laser probe and the microphone. This provides additional confirmation that the measured correlations have the desired physical origin rather than a stray electronic origin. Once the propagation time delay is confirmed, the frequency-domain plot of cross-spectral density is deemed superior to the time-domain correlation coefficient due to the additional frequency information. Therefore, all correlation data are presented here in terms of normalized cross-spectral density (coherence).

It is useful to point out that the present Rayleigh scattering based technique cannot measure density fluctuations associated with acoustic waves. The density fluctuations from the acoustic waves are at least 4 orders of magnitude below that from the turbulent flow, and therefore fall below the measurement noise floor. Sound generated from sources along the centreline has to propagate through the turbulent flow before emanating into the outside quiescent region. Since density fluctuations from this propagating part are too weak to be detected, the present technique only identifies the sound sources and excludes the propagating sound waves.

A comparative study of the correlation between turbulence fluctuations occurring along the peripheral shear layer and sound pressure fluctuations at $\theta = 30^\circ$ and $r = 50D$ for the three Mach number jets is shown in figure 15. There are remarkable differences between the three Mach number conditions. The coherence function lies in the noise floor for all measurement stations in the subsonic Mach 0.95 jet, indicating sound pressure fluctuations are uncorrelated to density fluctuations occurring in the shear layer. A very small rise above the noise floor is seen in the Mach 1.4 jet, particularly at $x/D = 6$ and 8, indicating a very weak correlation. Finally, the Mach 1.8 jet shows a significant rise above the noise floor, indicating a strong correlation between sound radiation and flow fluctuations at a frequency as high as $Sr = 1.8$.

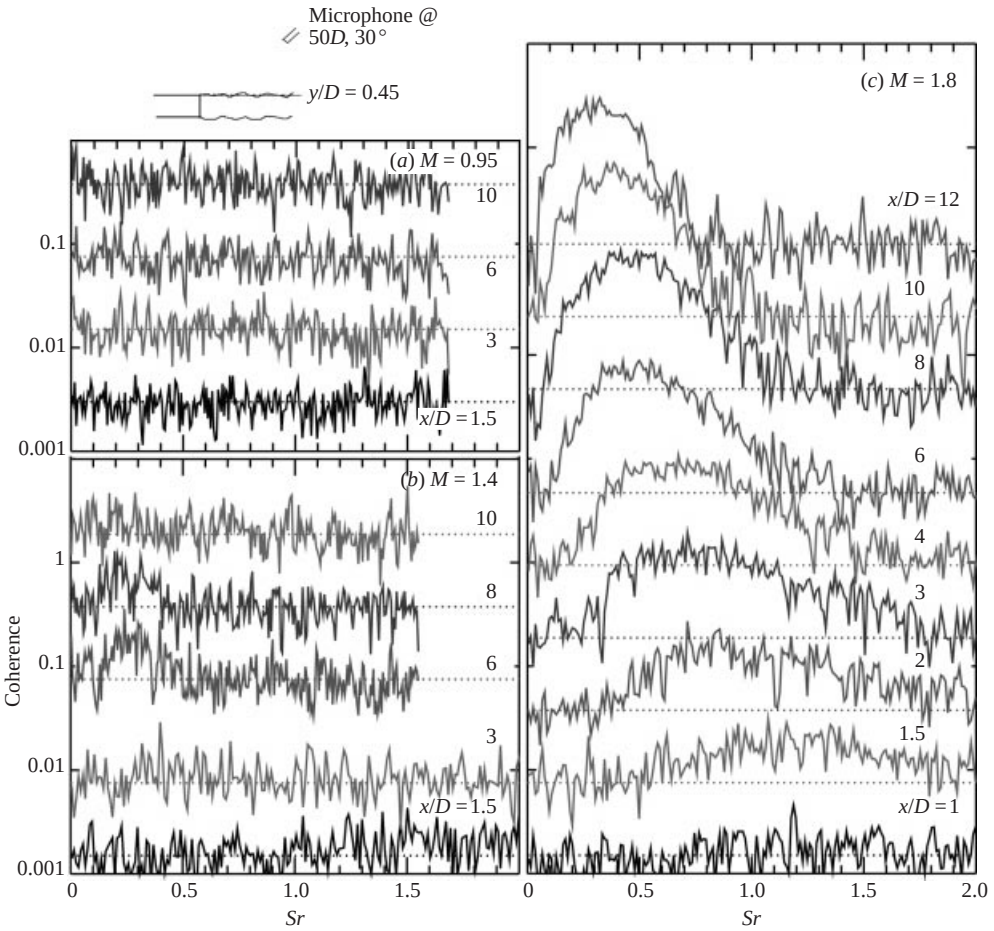

FIGURE 15. Normalized cross-spectrum between density and sound fluctuations from the three different jets. The microphone was fixed at $r/D = 50$, $\theta = 30°$ and the laser probe was moved to the indicated axial positions along the shear layer, $y/D = 0.45$. Dotted lines represent the noise floor of the measurement technique.

An interesting fact emerges when the shear layer correlation data of figure 15(*c*) are compared with the density fluctuations measured at similar positions – figure 10(*a*). The progressive lowering of peak frequency fluctuations with downstream distance and the general spectral shapes are remarkably similar for these two figures. Now, it has been established that the Kelvin–Helmholtz instability waves are responsible for the trends in the density fluctuation spectra. Therefore, it can be said that the same Kelvin–Helmholtz waves are directly responsible for noise generation in the Mach 1.8 jet. The Kelvin–Helmholtz waves are also clearly present in lower Mach number jets, yet they do not radiate noise. The reason lies in the difference of convection speed. The subsonic convection speed with respect to the ambient sound velocity precludes the instability waves from radiating noise via the Mach wave mechanism in the Mach 0.95 and 1.4 jets, while the supersonic speed in the Mach 1.8 jet makes it a efficient sound radiators.

The difference between the three jets is not as significant when the correlation data were measured from fluctuations occurring along the centreline, figure 16. A weak

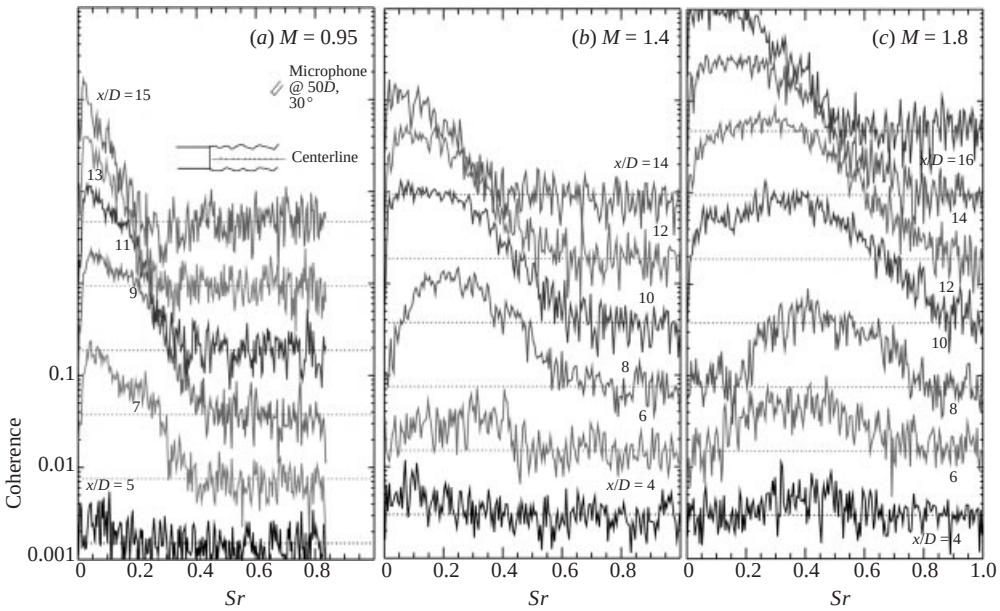

FIGURE 16. Normalized cross-spectrum between density and sound fluctuations from the three different jets. The microphone was fixed at $r/D = 50$, $\theta = 30^\circ$ and the laser position was moved to the indicated axial positions along the centreline.

or no correlation was measured until the laser probe was moved to the end of the potential core, beyond which a significant correlation in the low-frequency range ($Sr < 0.4$ for the Mach 0.95, $Sr < 0.8$ for the Mach 1.8) was measured in all Mach number jets. (Note that the centreline data are presented over a smaller frequency range than the preceding shear layer data.) The peak coherences are around 0.1 and occur somewhat downstream of the end of the potential core. The data show that the region downstream of the potential core is a low-frequency sound source for all Mach number jets, and such sources persist for many downstream diameters. To further verify the presence of these sources in subsonic jets, measurements were conducted at various low Mach number conditions (figure 17). That a measurable correlation can be found in the lowest Mach 0.6 jet indicates a subsonic sound generation mechanism different from the supersonic 'Mach wave' emission process. This subsonic sound generation process is present beyond the end of the potential core at all Mach number conditions. Figure 17 also shows that an increase in the jet Mach number cause an increase in both the magnitude and the frequency range of measurable coherence.

The spatial distribution of coherence values at different Strouhal frequencies for the Mach 0.95 and 1.8 jets are shown in the colour plots of figure 18. For this figure a large amount of correlation data was measured by moving the laser probe from point to point in the flow, while keeping the microphone location fixed. Later, coherence values at a desired Strouhal frequency were isolated for all measurement stations and plotted using the indicated colour scale. Note that the colour scale is such that the minimum value (green for $\Gamma = 0.005$) is above the noise floor ($\Gamma = 0.002$). Therefore regions of no or very low correlation are white. Since no correlation was measured in the Mach 0.95 jet for $Sr \geqslant 0.4$, coherence distributions at $Sr = 0.5$, 1 and 1.5 are not plotted. Once again, a clear distinction in measurable sound sources is visible

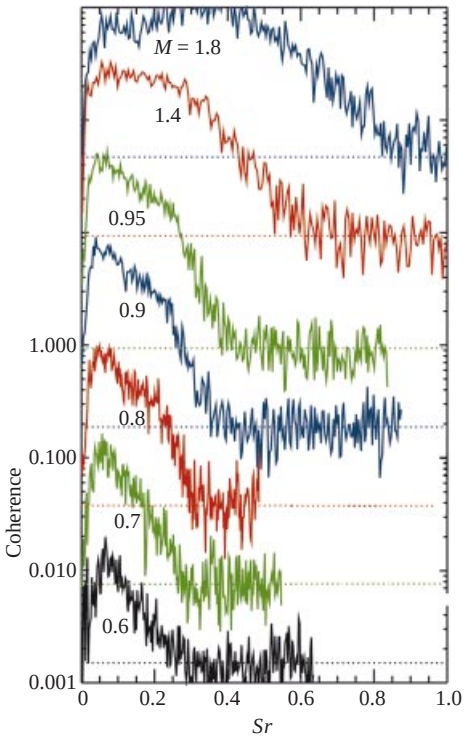

FIGURE 17. Normalized cross-spectrum between density and sound fluctuations from the indicated Mach number jets. Microphone was fixed at $r/D = 50$, $\theta = 30^\circ$ and the laser probe at the end of the potential core: centreline $x/D = 7$, 7.5, 7.5, 8, 8, 10 and 10 for, respectively, $M = 0.6$, 0.7, 0.8, 0.9, 0.95, 1.4 and 1.8 jets.

in figure 18. Density fluctuations causing sound generation up to $Sr = 1.5$ could be determined only in the Mach 1.8 jet; the higher frequency source lies closer to the nozzle exit. The lower frequency source in both jets is strongest along centreline, after the end of potential core. Such sources weaken rapidly in the radial direction and very slowly in the downstream direction. An additional utility of figure 18 is that it provides an answer to the non-uniqueness issue inherent in the causality method of source identification. Ffowcs Williams (1973) has provided a detailed discussion of this problem. In brief, since the sound pressure fluctuation is a sum of contributions from everywhere in the flow, many different distributions of flow–sound correlation can produce the same mean-square pressure fluctuation at the microphone location. Among all possible distributions, the physically plausible distribution is the correct solution. Figure 18 provides this physically measurable correct distribution.

The bulk of the correlation study was performed with a fixed microphone position of $r = 50D$ and $\theta = 30^\circ$, the peak noise emission angle. The dependence of the correlation data on radial distance was explored by moving the microphone to various radial positions, keeping its angular position θ and all other variables constant. Figure 19 shows a nearly unchanging coherence for $r/D = 25$, 50 and 75, which indicates that the microphone is effectively in the acoustic far field of the jet. The correlation data are expected to vary significantly with the microphone angular position, θ . This angular dependence was not studied in the present work except for limited data for $\theta = 90^\circ$. At this angular position, the microphone was significantly more affected by acoustic

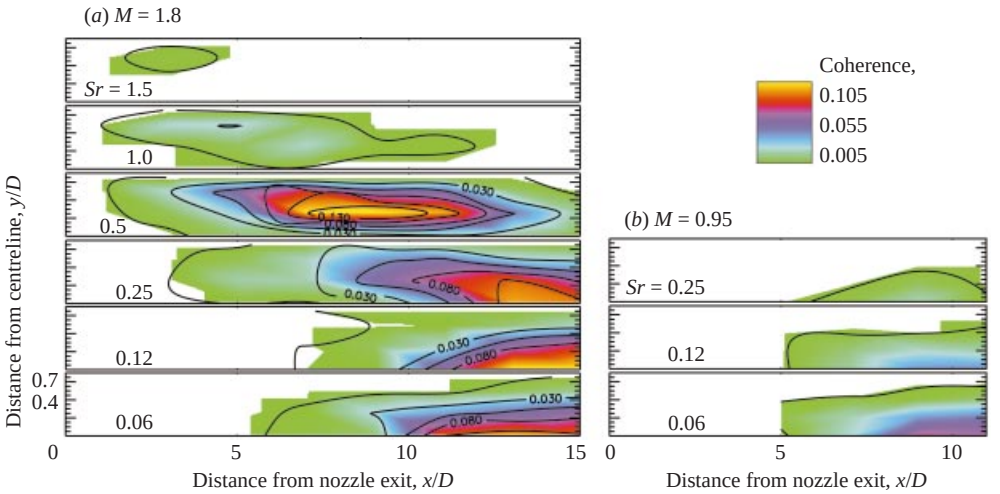

FIGURE 18. Distribution of normalized cross-spectrum between flow density and far-field sound pressure fluctuations at the indicated Strouhal frequencies for two different jets. The microphone was fixed at $r/D = 50$, $\theta = 30^\circ$ while the laser probe was moved.

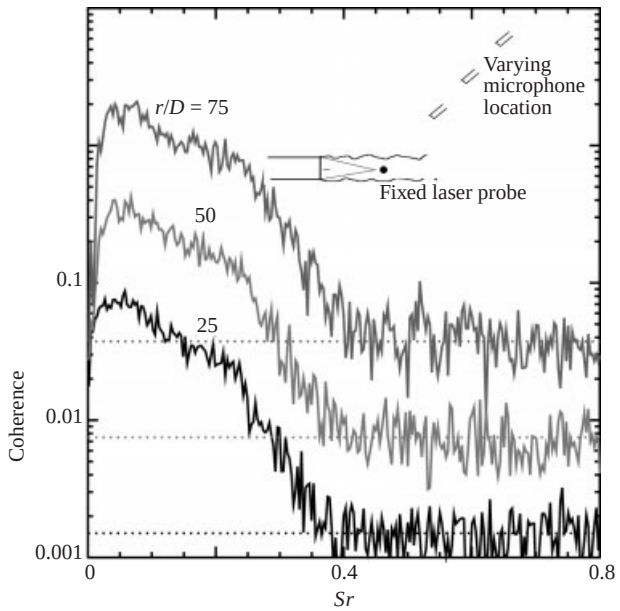

FIGURE 19. Normalized cross-spectrum between density and sound fluctuations in the Mach 0.95 jet. The laser probe was fixed at the centreline and $x/D = 8$, while the microphone was moved to the indicated radial positions along $\theta = 30^\circ$. The sketch is not to scale.

reflection from the uncovered optical elements, beam dump and the uncovered part of the jet facility. In turn, the flow–sound correlation was also affected. Figure 20 presents some data obtained for the Mach 1.8 jet. A comparison with corresponding data from the 30° microphone (figure 16*c*) shows a significant decrease in the level and spread of correlation. Additional data measured for the Mach 1.4 jet (not shown) showed an even larger decrease. In fact, no correlation was measured between the

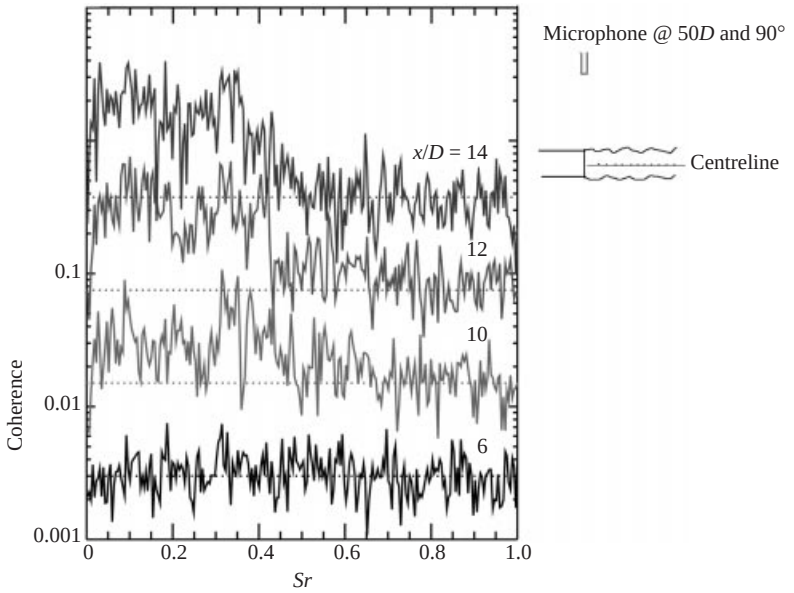

FIGURE 20. Normalized cross-spectrum between density and sound fluctuations in the Mach 1.8 jet. The microphone was fixed at $r/D = 50$, $\theta = 90^\circ$ and the laser position was moved to the indicated axial positions along the centreline.

density fluctuations occurring anywhere in the Mach 0.95 jet and sound pressure fluctuations at the 90° location.

Finally, a comparison with the earlier experimental data on sound source location, obtained through the causality principle, shows a mixed outcome. Almost all earlier studies were performed in subsonic jets, and therefore, the distinct difference between the subsonic and supersonic conditions was not observed. The subsonic jet studies were conducted with a microphone placed at the peak 'shear noise' location, nominally $\theta = 30^\circ$, similar to the present experiment. The maximum coherence between sound pressure fluctuations at the microphone location and velocity fluctuations in either the Mach 0.3 jet (measured using hot-wires, Seiner & Reethof 1974) or the Mach 0.9 jet (measured using laser Doppler velocimetry by Schaffer 1979) was found to be about 0.1, in agreement with the present data. The peak value was also measured from the end of the potential core and at the centreline. However, the distribution of coherence differed significantly from the present experiment. Unlike the present, experiment, significant correlation was measured from the thin peripheral shear layer at the early part of jet development. The two-microphone correlation technique of Armstrong *et al.* (1977) similarly showed that in a subsonic Mach 0.5 jet the axial location of peak turbulence fluctuation of a given Strouhal number is also the location for peak correlation with noise at that frequency. This demonstrates an important non-conformance of the present data with an existing belief of sound generation from instability waves. Since higher frequency instability waves peak closer to the nozzle exit, the existing belief is that slices of the jet lying closer to the nozzle will emit higher frequency sound waves in the downstream direction for all jet Mach numbers. The present experiment confirms this belief for jets where instability waves attain supersonic speed relative to the ambient sound speed and disproves it for subsonic conditions.

4. Summary and conclusion

This paper presents an improved technique to measure air density fluctuations from Rayleigh scattered light, an application of this technique to map turbulent fluctuation spectra and finally a relationship between the flow density fluctuations and the far-field noise. The flows under study are unheated plumes in the Mach number range $0.5 \leqslant M \leqslant 1.8$.

The fundamental superiority of the Rayleigh scattering technique compared to the traditional hot-wire technique, laser Doppler velocimetry or particle image velocimetry lies in its non-intrusiveness – the ability to obtain information directly from the gas molecules (no seed particles are used). The major source of uncertainty in calculating density through measuring scattered light intensity is due to electronic shot noise. A significant part of the paper is devoted to presenting the experimental technique, various means to reduce the contribution from electronic shot noise, and uncertainty estimates. The Rayleigh scattered light from a point in the flow was measured using photomultiplier tubes and photon counting electronics. The counting was performed on a large number of contiguous bins of small time duration. An average of all counts provided a measure of time-averaged density. Subtraction of the average from the mean-square provided measurement of mean-square density fluctuations. The spectral information on density fluctuations was gathered by dividing the collected light into two parts, measuring individual intensities using two sets of PMT and photon counting electronics and finally cross-correlating the two time signals. Since electronic shot noise from the two PMTs is uncorrelated, the cross-correlation process significantly reduces its contribution. Finally, to determine the sound sources a 'causality approach' was followed where acoustic pressure signal from a microphone, placed in the far noise field, was correlated with the Rayleigh light to determine the portion of the density fluctuations radiating to the far field.

Time-averaged density measurements, obtained from radial and centreline surveys, confirmed expected trends such as a slow down of jet spread with an increase in Mach number. The root-mean-square fluctuation, normalized by the difference between jet and ambient density $\rho_{rms}/(\rho_j - \rho_a)$, was found to peak in the shear layer and fall to the noise floor in the quiescent core. The peak fluctuation was measured to be about 0.22 and was in agreement with previous measurements of Wilson & Damkevala (1970). The centreline surveys showed the existence of weak shock-cell structures inside the pressure-matched supersonic jets. The time-averaged schlieren photographs confirmed this observation.

The density fluctuation spectra provide footprints of the turbulence fluctuations present in jets. The source of fluctuation is mixing between cold, high-density air from the primary jet and warm, low-density ambient air. In order to compile a database for computational fluid dynamic simulations, density spectra were measured at a large number of points in the flow. When frequency values were normalized to Strouhal numbers, and spectral density values were divided by the difference of jet and air densities, the fluctuations appeared remarkably similar in all three jets. Even the distribution of various Strouhal frequency components was similar. The only difference was a spatial stretching with an increase in the Mach number. The distributions followed the expected behaviour of Kelvin–Helmholtz instability waves. The high-Strouhal-frequency fluctuations were most energetic in the initial thin shear layer. As the shear layer thickened further downstream, the spectral peaks moved to lower Strouhal numbers.

The majority of correlation measurements between air density fluctuations and far-field sound pressure fluctuations were performed with a microphone fixed at

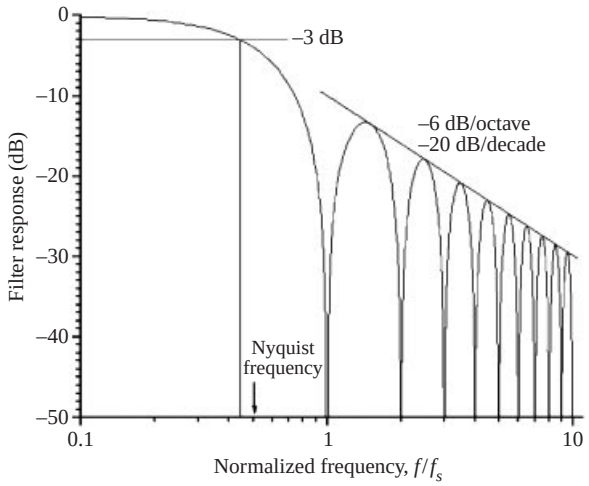

FIGURE 21. Response of integrate and dump filter.

the peak noise emission angle of 30° to the jet axis and 50 diameters from the nozzle exit. The laser probe volume was moved from point to point in various Mach number plumes. Detailed maps of the normalized cross-spectral density (coherence, Γ) function at different Strouhal frequencies were obtained in Mach 1.8 and 0.95 plumes. In general, two different regions could be identified as sound sources: the peripheral shear layer around the potential core and a long region downstream of the potential core. The former behaves differently in the two jets while the latter shows similarity. Density fluctuation from the peripheral shear layer is found to be well correlated with sound pressure fluctuation for $Sr \leqslant 1.5$ in the Mach 1.8 jet and uncorrelated at all Strouhal frequencies in the Mach 0.95 jet. It was established that this difference was caused by the presence or absence of the Mach wave radiation process from the Kelvin–Helmholtz instability waves. The Kelvin–Helmholtz instability waves were convected at supersonic speed relative to the ambient media in the Mach 1.8 jet and, therefore, produced significant sound radiation in the microphone direction, while a subsonic convection speed in the Mach 0.95 jet prohibited this process. Air density fluctuations from the second region, downstream of the potential core, were found to be a universal low-Strouhal-frequency sound source for all Mach number jets down to the lowest Mach 0.6 case tested. This perhaps indicates the presence of a subsonic sound generation mechanism, different from the Mach wave emission process. The low-frequency ($0 \leqslant Sr \leqslant 0.8$ for the Mach 1.8 jet, $0 \leqslant Sr \leqslant 0.4$ for the Mach 0.95 jet) source is found to be strongest at the centreline and at the end of the potential core, and decays quickly in the radial direction while persisting for a long downstream distance. The present correlation measurement technique could not identify higher frequency, $Sr \geqslant 0.4$, sound sources in subsonic plumes.

The authors acknowledge fruitful discussions with Dr Khairul Zaman and Dr Milo Dahl of NASA Glenn Research Center.

Appendix. Integrating filter frequency response

Consider a sinusoidal input signal of frequency $f, S_i(f) = A\sin(2\pi f t)$, passed through an integrating filter (integrate-and-dump filter), where the signal is integrated

over time interval Δt. The output S_o of the filter (including a gain of $1/\Delta t$), sampled once per integration interval is

$$S_o(f) = \frac{1}{\Delta t}\int_{t-\Delta t/2}^{t+\Delta t/2} S_i(t')\,\mathrm{d}t' = \frac{A}{\pi f \Delta t}\sin(2\pi f t)\sin(2\pi f \Delta t/2).$$

The transfer function of the filter is thus

$$H(f) = \frac{S_o(f)}{S_i(f)} = \frac{\sin(\pi f \Delta t)}{\pi f \Delta t}.$$

Since the sampling frequency $f_s = 1/\Delta t$, the transfer function becomes

$$H(f) = \frac{\sin(\pi f/f_s)}{\pi f/f_s}$$

A plot of this function is shown in figure 21. The 3 dB point occurs at $f/f_s = 0.44$ and the response falls to zero at an integral multiple of the sampling frequency. This shows that an integrate-and-dump filter passes some signal at frequencies greater than the Nyquist frequency $f/f_s = 0.5$.

REFERENCES

Armstrong, R. R., Michalke, A. & Fuchs, H. V. 1977 Coherent structures in jet turbulence and noise. *AIAA J.* **15**, 1011–1017.

Bishop, K. A., Ffowcs Williams, J. E. & Smith, W. 1971 On the noise sources of the unsuppressed high-speed jet. *J. Fluid Mech.* **50**, 21–31.

Colonius, T., Lele, S. K. & Moin, P. 1997 Sound generation in a mixing layer. *J. Fluid Mech.* **330**, 375–409.

Crow, S. C. & Champagne, F. H. 1971 Orderly structure in jet turbulence. *J. Fluid Mech.* **48**, 547–591.

Damkevala, R. J., Grosche, F. R. & Guest, S. H. 1973 Direct measurement of sound sources in air jets using the crossed beam correlation technique. *Noise Mechanisms AGARD CP* 131, pp. 3-1 to 3-16.

Ffowcs Williams, J. E. 1963 The noise from turbulence convected at high speed. *Phil. Trans.* A **255**, 469–503.

Ffowcs Williams, J. E. 1973 Technical evaluation report. *Noise Mechanisms, AGARD CP* 131, VII–XIX.

Freund, J. B. 2001 Noise sources in a low-Reynolds-number turbulent jet at Mach 0.9. *J. Fluid Mech.* **438**, 277–305.

Gouldin, F. C. & Halthore, R. N. 1986 Rayleigh scattering for density measurements in premixed flames. *Expts. Fluids* **4**, 269–278.

Hurdle, P. M., Meecham, W. C. & Hodder, K. 1974 Investigation of the aerodynamic noise generating region of a jet engine by means of the simple source fluid dilatation model. *J. Acoust. Soc. Am.* **56**, 1708–1721.

Hussain, A. K. M. F. & Clark, A. R. 1977 Upstream influence on the near field of a plane turbulent jet. *Phys. Fluids* **20**, 1416–1426.

Jiang, L. Y. & Sislian, J. P. 1998 Velocity and Density measurements in supersonic high-temperature exhaust plume. *AIAA J.* **36**, 1216–1222.

Lau, J. C. 1981 Effects of exit Mach number and temperature on mean flow and turbulence characteristics in round jets. *J. Fluid Mech.* **105**, 193–218.

Lee, H. K. & Ribner, H. S. 1972 Direct correlation of noise and flow of jet. *J. Acoust. Soc. Am.* **52**, 1280–1290.

Liepmann, H. W. & Roshko, A. 1958 *Elements of Gasdynamics*. John Wiley.

Lighthill, M. J. 1954 On sound generated aerodynamically I. General theory. *Proc. R. Soc. Lond.* A **221**, 564–587.

Lilley, G. M. 1972 The generation and radiation of supersonic jet noise IV. Theory of turbulence generated noise. *USAPL TR*-72-53.

Lowson, M. V. & Ollerhead, J. B. 1968 Visualization of noise from cold supersonic jets. *J. Acoust. Soc. Am.* **64**, 624–630.

McLaughlin, D. K., Morrison, G. L. & Troutt, T. R. 1975 Experiments on the instability waves in supersonic jets and their acoustic radiation. *J. Fluid Mech.* **69**, 73–95.

Michalke, A. 1970 A wave model for sound generation in circular jets. *DLR Rep.* FB 70-57.

Michalke, A. 1972 An expansion scheme for the noise from circular jets. *Z. Flugwissensch.* **20**, 229–237.

Mollo-Christensen, E. 1967 Jet noise and shear flow instability seen from an experimenter's viewpoint. *Trans. ASME J. Appl. Mech.* **89**, 1–7.

Moore, C. J. 1977 The role of shear-layer instability waves in jet exhaust noise. *J. Fluid Mech.* **80**, 321–367.

Morris, P. J. & Tam, C. K. W. 1979 On the radiation of sound by the instability waves of a compressible axisymmetric jet. In *Mechanisms of Sound Generation in Flows* (ed. E. A. Muller). Springer.

Morrison, G. L. & McLaughlin, D. K. 1979 Noise generated by instabilities in low Reynolds number supersonic jets. *J. Sound Vib.* **65**, 177–191.

Panda, J. & Seasholtz, R. G. 1999*a* Velocity and temperature measurement in supersonic free jets using spectrally resolved Rayleigh scattering. *AIAA Paper* 99-0296.

Panda, J. & Seasholtz, R. J. 1999*b* Measurement of shock structure and shock-vortex interaction in underexpanded jets using Rayleigh scattering. *Phys. Fluids* **11**, 3761–3777.

Papamoschou, D. 1997 Mach wave elimination in supersonic jets. *AIAA J.* **35**, 1604–1611.

Philips, O. M. 1960 On the generation of sound by supersonic turbulent shear layers. *J. Fluid Mech.* **9**, 1–28.

Pitts, W. M. & Kashiwagi, T. 1984 The application of laser-induced Rayleigh scattering to the study of turbulence mixing. *J. Fluid Mech.* **141**, 391–429.

Proudman, I. 1952 The generation of noise by isotropic turbulence. *Proc. R. Soc. Lond.* A **214**, 119–132.

Richarz, W. G. 1979 Direct correlation of noise and flow of a jet using Laser Doppler. *AIAA Paper* 79-0571.

Saleh, B. E. A. & Teich, M. C. 1991 *Fundamentals of Photonics.* John Wiley.

Schaffer, M. 1979 Direct measurements of the correlation between axial in-jet velocity fluctuations and far field noise near the axis of a cold jet. *J. Sound Vib.* **64**, 73–83.

Seasholtz, R. G. & Panda, J. 1999 Multiple point dynamic gas density measurements using molecular Rayleigh scattering. *NASA TM* 1999-209295.

Seasholtz, R. G., Zupanc, F. J. & Schneider, S. J. 1992 Spectrally resolved Rayleigh scattering diagnostic for hydrogen-oxygen rocket plume studies. *J. Propulsion Power* **8**, 935–942.

Seiner, J. M. & Reethof, G. 1974 On the distribution of source coherency in subsonic jets. *AIAA Paper* 74-4.

Siddon, T. E. & Rackl, R. 1972 Cross-correlation analysis of flow noise with fluid dilatation as source fluctuation, *J. Acoust. Soc. Am.* **51**, 96(A).

Smits, J. A. & Dussauge, J.-P. 1996 *Turbulent Shear Layers in Supersonic Flow*. AIP Press.

Tam, C. K. W. & Burton, D. E. 1984 Sound generated by instability waves of supersonic flows. Part 2. Axisymmetric jets. *J. Fluid Mech.* **138**, 249–271.

Welch, P. D. 1967 The use of fast Fourier transform for the estimation of power spectra: A method based on time averaging over short, modified periodograms. *IEEE Trans. Audio Electroacoust.* **AU-15**, 70–73.

Wilson, L. N. & Damkevala, R. J. 1970 Statistical properties of turbulent density fluctuations. *J. Fluid Mech.* **43**, 291–303.

Yu, J. C. & Dosanjh, D. S. 1972 Noise field of a supersonic Mach 1.5 cold model jet. *J. Acoust. Soc. Am.* **51**, 1400–1410.

Zaman, K. B. M. Q. 1986 Flow field and near and far sound field of a subsonic jet. *J. Sound Vib.* **106**, 1–16.